A Model-based Fault Detection Method for the Position Transducer in the Ampelmann System.

E. M. Claassen

WWW.AMPELMANN.NL

TUDelft Delft University of Technology

Delft Center for Systems and Control

A Model-based Fault Detection Method for the Position Transducer in the Ampelmann System.

MASTER OF SCIENCE THESIS

For the degree of Master of Science in Systems and Control at Delft University of Technology

E. M. Claassen

May 2, 2018

Faculty of Mechanical, Maritime and Materials Engineering (3mE) · Delft University of Technology

TUDelft Delft University of Technology

DCSC

DELFT UNIVERSITY OF TECHNOLOGY
DEPARTMENT OF
DELFT CENTER FOR SYSTEMS AND CONTROL (DCSC)

The undersigned hereby certify that they have read and recommend to the Faculty of Mechanical, Maritime and Materials Engineering (3mE) for acceptance a thesis entitled

A MODEL-BASED FAULT DETECTION METHOD FOR THE POSITION TRANSDUCER IN THE AMPELMANN SYSTEM.

by

E. M. CLAASSEN

in partial fulfillment of the requirements for the degree of

MASTER OF SCIENCE SYSTEMS AND CONTROL

Dated: <u>May 2, 2018</u>

Supervisor(s):

_____
Prof.dr.ir. J.W. van Wingerden

_____
Ir. J.J. Flohil

Reader(s):

_____
Dr. R.M.G. Ferrari

_____
V. Rostampour

Abstract

The Ampelmann system offers a safe and reliable solution for offshore access. As safety is a key factor, an extensive safety and warning management system is employed which accommodates for different fault types that may occur. Accommodation of sensor failure in the Ampelmann system is currently done through switching to a redundant component. However, there are several faults that are left undetected in the system. Detection only occurs when the faults exceed a critical threshold. Exceeding this threshold immediately results in shut-down of the system as safety is no longer guaranteed. For sensor equipment critical to the motion compensation, this leads to a code black in the system. The occurrences of code blacks should be limited where possible due to the fact that these lead to downtime.

A critical sensor for the motion control is the position transducer in the hydraulic cylinders. The measured lengths are used for feedback purposes in the control system. The position transducer is redundant in each cylinder. The redundant sensor is mainly utilized for checking the main sensor. However, when the measurements from both sensors deviate too much from one another the system will shut down.

Therefore, in this thesis, the possibility of a model-based fault detection method for the position transducer in the hydraulic cylinder is explored. Firstly, an accurate model of the hydraulic cylinder is derived and identified. Then, the model is combined with an observer to generate accurate estimates of the cylinder lengths. Furthermore, the estimates are compared with the actual measured cylinder lengths from the position transducer to generate residuals. Finally, the residuals are evaluated in order to make a decision about the health of the sensor.

Three different fault types have been defined, which are expected to cause sensor degradation/failure. For each fault type, the residuals are evaluated. Prior to this a threshold has been defined based on a fault-free case. The threshold determines whether the system is healthy or not. Ideally, when there is no fault in the system, the residual is close to zero. Whereas, when there is a fault present the residual will be much larger. Whenever the threshold is exceeded, the detection system knows that there is a fault present, which allows it to sent out a warning. There are three model-based fault detection estimators which generate three different residuals. These three estimators are combined into one fault detection architecture.

The results developed throughout this thesis have provided new insights for the fault monitoring system in the Ampelmann system. Currently it has only been applied for the position transducer. However, it can be extended to other critical components in the system. Furthermore, the work presented in this thesis is valuable for predictive maintenance purposes. Finally, the detection estimators can be used for the implementation of fault tolerant control in the system.

Table of Contents

List of Figures

List of Tables

Acknowledgements

During the last 12 months, I had the chance to work on a interesting and challenging graduation project at an amazing company. I hereby would like to thank everyone who has made this project into a success.

First of all, I would like to thank prof. dr. ir. Jan-Willem van Wingerden from the Delft University of Technology for his supervision. The guidance and feedback during the monthly meetings were very insightful.

Furthermore I would like to thank Jasper Flohil and Jeroen van Rooijen for their daily supervision at Ampelmann. Their ideas and creative input on the research have really helped developing the work and kept it in the right direction.

Finally, I would like to thank my family for granting me this opportunity and my friends for supporting me throughout this process. A special thanks to those who have read (parts) of this thesis. Their input has been really valuable.

Delft, University of Technology   E. M. Claassen
May 2, 2018

Chapter 1

Introduction

Offshore structures such as offshore windmills and oil & gas platforms need regular access for operations and maintenance. However, the accessibility of said structures depends largely on the weather conditions. Transferring people from a vessel to a platform can become unsafe due to vessel motion caused by rough weather conditions. In 2009, the Ampelmann system offered a safe solution to offshore access; making it *as easy as crossing the street* [1]. They designed a ship-based, self-stabilizing transfer platform with a gangway attached to it to safely transfer people offshore, Figure 1-1.

Figure 1-1: Ampelmann E-type during offshore operation

In order to offer a safe solution for offshore access, a reliable system is required. Hence, the system is closely monitored for any possible faults during operation. A monitoring and alarm system will ensure that any detected failure or fault will trigger a corresponding warning and action. Fault accommodation is done through switching to a redundant component. However, in the current warning system, there are some alarms which will lead to immediate

shut-down of the operation because safe operation is no longer guaranteed. The reason for this is that both the main and redundant component are failing. Another reason is that no proper decision can be made about the location of the fault, the main component or the redundant one. For sensors critical to the motion compensation of the hexapod, this type of alarm is referred to as a code black in the system. Ideally, the occurrence of these alarms should be limited as they will lead to downtime.

A short introduction to the Ampelmann system and fault detection is presented in the following sections.

1-1   The Ampelmann System

The Ampelmann system that will be considered in this thesis is the Ampelmann E-type, Figure 1-2. The Ampelmann E-Type, which is the largest system available, is especially engineered for rough weather conditions and to be able to carry large weight.
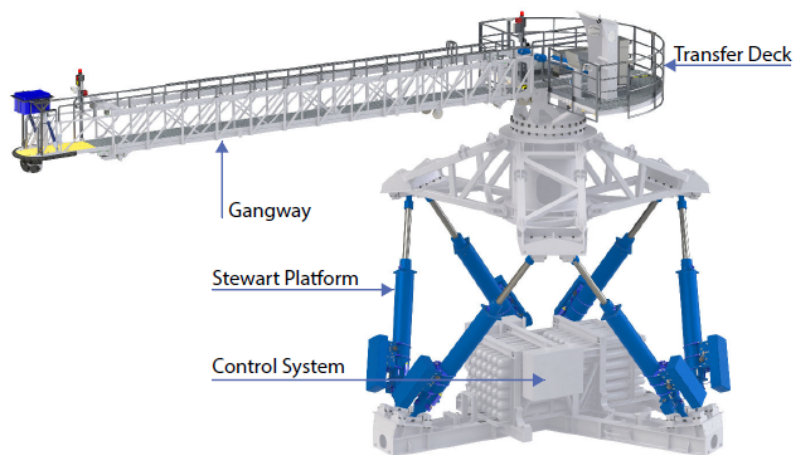
Figure 1-2: The Ampelmann E-type System

The system can compensate for six Degrees of Freedom (DoF) using the Stewart platform. The Stewart platform consists of six hydraulic actuators that are connected to a base and top frame. On top of the top frame, a transfer deck and gangway are placed. The control system will calculate the reference lengths and velocities for the six cylinders such that the transfer deck will remain motionless.

The Ampelmann system has four different platform states to ensure safe operation [1]. When an emergency condition occurs, the system will switch to safe mode from any of the other three states, Figure 1-3. This happens within a matter of seconds. During a code black, the motion is hardware controlled and thus the cylinders do not operate smoothly at equal velocities. Therefore, when the system switches from engaged to safe mode this can feel uncomfortable to people on the Ampelmann system.
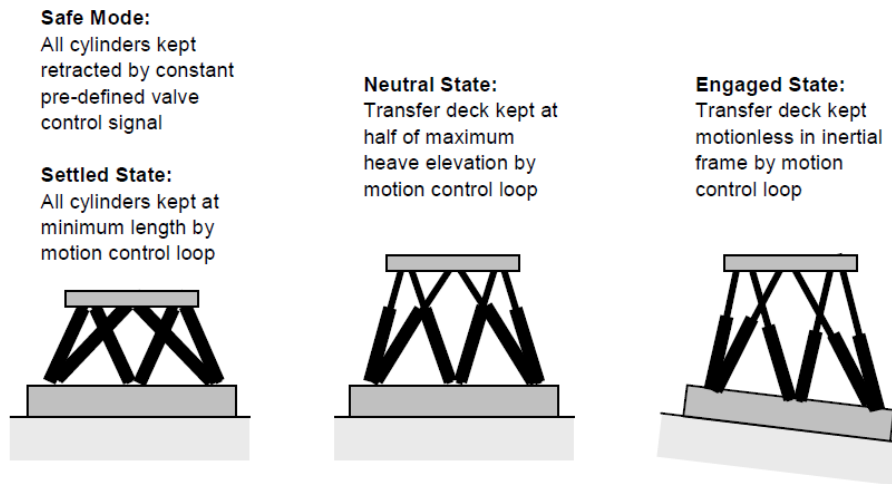
Figure 1-3: The different states of the Ampelmann system [1]

Current alarm system

Currently, all critical sensors in the Ampelmann system are redundant. This physical redundancy can give assurance on the proper operation of the sensors and thus increases reliability of their measurements. Sensor faults can be categorized into three different categories:

- **Broken wire:** there is no incoming signal from the sensor.

- **Out of range:** the incoming signal is not realistic.

- **Difference too big:** the difference between the incoming signal and the redundant signal exceeds a pre-defined threshold.

The first two can easily be checked and accommodated for with the redundant sensor. The third type of fault, however, is where the real challenge lies. With the duplex physical redundancy, no decision can be made about the reliability of the sensor measurement when it differs too much from the redundant measured value. In order to make a decision, triplex physical redundancy is required. As this fault cannot be accommodated with the redundant sensor, the system will either give a code black or a code red and switch to safe mode: black when it concerns a sensor critical to the motion compensation and red when the sensor is not critical for the motion compensation.

1-2   Fault Detection

Fault detection and accommodation have gained a lot of interest over the past few decades [5]. Detection concerns itself with the different approaches of detecting faults in a system. Accommodation concerns itself with the redesign of control such that it becomes adaptable to the fault. This thesis will solely focus on the detection part. As systems have become more complex, monitoring every part has become a challenge on its own. One of the approaches used

is a form of analytical redundancy. Analytical redundancy is a model-based fault detection approach that relies on an accurate mathematical model to estimate the variables that need to be checked. These estimates and the actual values generate residuals. The residuals will be evaluated to make a decision on whether a specific component is healthy or faulty.

1-3   Problem Statement

During normal operation, the Ampelmann system will always go from engaged to neutral to settled before going into safe mode. For that reason going immediately from engaged mode to safe mode is not desired, and the number of times this happens should be limited if possible. When the two position transducers that measure the cylinder length give the alarm of "Difference too big", the system will give a code black and go into safe mode. In that case the physical redundancy is not sufficient enough to guarantee safe operation. This can be solved by implementing a third sensor. However, the downside of triple physical redundancy is that it results in extra components, which means an increase in costs and complexity of the system.

This means that, in order to increase measurement reliability, it is beneficial to investigate an alternative solution.

1-4   Objectives

From the problem statement in Section 1-3 it follows that duplex physical redundancy for the position transducers is not sufficient in all cases. Therefore, the main goal of this thesis is to achieve an extra analytical redundancy measure for the position transducers in the Ampelmann system.

Goal: Increasing reliability of the position measurements and thus reducing downtime of the Ampelmann system by implementing a model-based fault detection method.

In this thesis, the focus lies on one of the critical sensors in the system: the position transducers in the hydraulic cylinders that measure the lengths and velocities of the cylinders. The relevance of this sensor to the system is that the control strategy relies on correct feedback of the cylinder lengths. Thus a failure or fault in the position transducer will have a big impact on the operation of the system.

In order to achieve this goal, the following three questions are posed to guide the research.

Question 1: Can an accurate model of the hydraulic cylinders be derived that can be used for the model-based fault detection method?   The model-based fault detection method requires an accurate model. The model should be derived such that it captures the dynamics of the hydraulic cylinder in terms of position and velocity.

Question 2: Using the model from Question 1, can a model-based estimator be designed such that it gives accurate estimates of cylinder lengths?   This model-based estimator will be used to generate residuals. The accuracy of the estimates determines with what accuracy faults can be detected.

Question 3: What types of faults can be expected to occur in the sensor that will lead to a "Difference too big"?   There are different kinds of faults that can occur in the sensor that will result in small changes in the measurements. Their effects on the residual may vary and therefore should all be considered.

1-5   Outline of the Report

This thesis is structured in such a manner that the questions in Section 1-4 are answered in a logical sequence. However, firstly in Chapter 2, the Ampelmann system and its control strategy will be explained. In order to answer Question 1, in Chapter 3 and Chapter 4, an accurate mathematical model is derived, identified, and validated. Next, in Chapter 5, the answers to Question 2 and 3 will be provided by introducing a model-based fault detection strategy for the position transducer. Finally, Chapter 6 synthesizes the work presented in this thesis. Furthermore, recommendations for future research are presented.

Chapter 2

The Ampelmann System

In this chapter, the Ampelmann system will be discussed, with a predominant focus on its safety design. The Ampelmann system is designed to be fail-operational [1]. This means that when a single component fails, it should be able to continue operation by using a redundant component. Thus when looking at the motion control loop in Section 2-1 it will be shown that all safety-critical components are redundant. Furthermore, in Section 2-2, the current Ampelmann Safety Management System (ASMS) is explained.

2-1   The Control System

As previously mentioned in Chapter 1, the system can compensate for the six Degrees of Freedom (DoF) of a vessel. The six DoF of a ship are defined as shown in Figure 2-1.
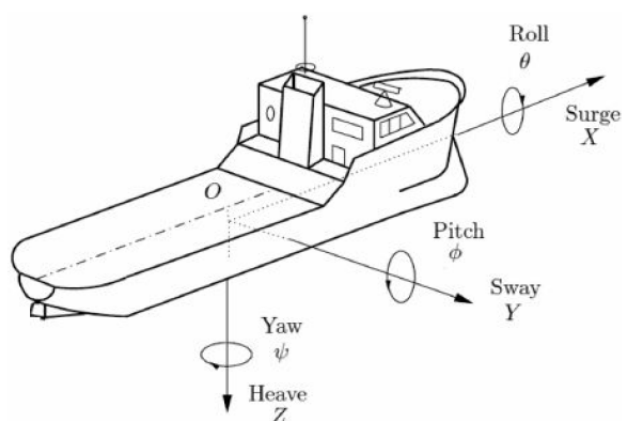
Figure 2-1: The six degrees of freedom of a vessel

Vessel motions are measured and translated into desired reference lengths and velocities of the six Stewart platform cylinders in such a way that the top platform stays virtually motionless.

A Motion Reference Unit (MRU) measures the vessel motions. The MRU measurements are sent to a controller. The controller computes the desired cylinder positions from the MRU measurements. The reference signal is combined with the feedback from the sensors in the cylinders and translated into a control signal for the actuators. The control signal is such that the platform on top of the actuators stays motionless.

In Figure 2-2 a simplified block scheme of the different components that measure (red), control (blue) or actuate (green) the system is given. Furthermore, it shows all the safety critical components as redundant components.
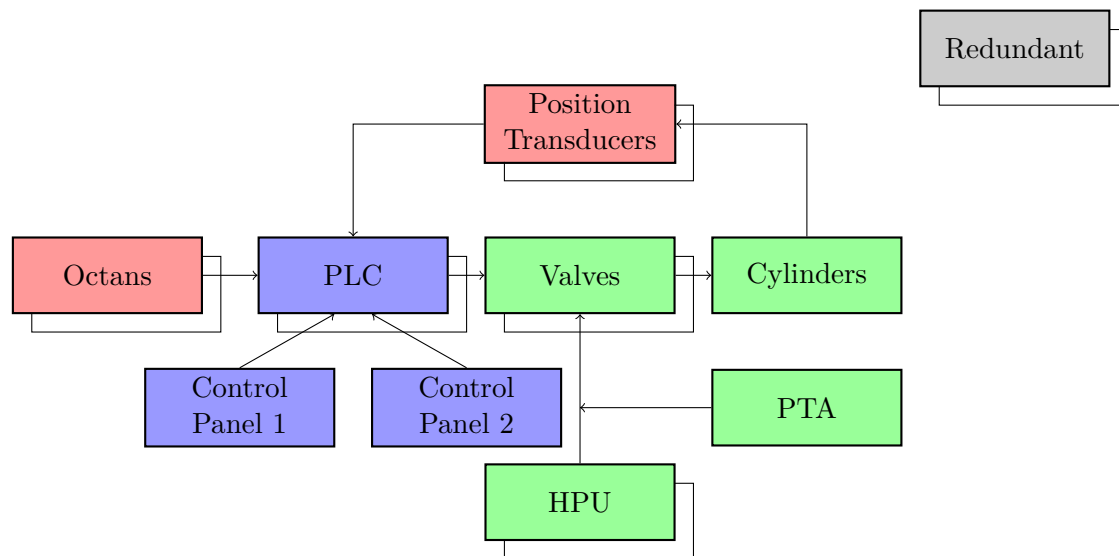
Figure 2-2: Simplified block scheme of the system and its redundant components.

Octans Motion Sensor

The vessel motions are measured using an Octans Fibre Optic Gyroscope produced by iXSea. The Octans motion sensor measures the rotational velocities - $\dot{\varphi}$, $\dot{\theta}$, $\dot{\psi}$ - using three fibre optic gyroscopes. These rotational velocities are integrated to determine the rotations - φ, θ, ψ. Using three accelerometers, the translational accelerations of the vessel are measured, - $\ddot{x}$, $\ddot{y}$, $\ddot{z}$. Integrating the accelerations once gives the translational velocities - $\dot{x}$, $\dot{y}$, $\dot{z}$ - and integrating twice gives the translations - x, y, z.

Position Transducers

The position transducers measure the lengths of the cylinders. These measurements are required for control purposes and should therefore always be available. The position transducers are placed inside the hydraulic cylinders. For this reason, replacing such a sensor is difficult, because the entire cylinder needs to be taken out of the system.

Programmable Logic Controller

The Programmable Logic Controller (PLC) receives the measurements from the Octans, the position transducers and the operator input from the control panels. In Figure 2-3, a schematic overview of the control module for a single actuator in the PLC is shown.
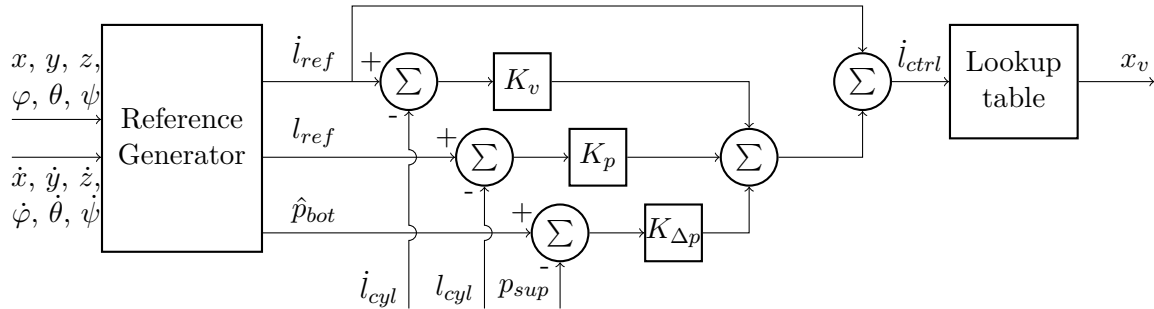
Figure 2-3: Control module for a single hydraulic actuator

The reference generator will calculate the desired reference lengths and velocities for the hydraulic cylinders such that the Ampelmann system compensates for the vessel motions. The lengths and velocities can be found through solving the Inverse Kinematics (IK) problem. If the Stewart platform is assumed in a certain pose and the position and orientation of both the top and bottom platform are known, it is possible to calculate the corresponding actuator lengths using IK [6]. Furthermore, when the rotational and translational velocities of the top and bottom platform are known, then the actuator velocities can be calculated as well using IK. For a more elaborate explanation of the IK problem see Appendix A. Moreover, the lengths and velocities of the cylinders are limited due to the workspace of the system [7]. The control module employs a combination of velocity feed-forward as well as position, velocity and pressure feedback [8]. This results in a control speed $\dot{l}_{ctrl}$. This control signal is sent through a look-up table to obtain the corresponding valve spool position. The lookup table maps the desired control velocity of the cylinder to the corresponding valve position. It accounts for the non-linearities in the valve. Motion tests are completed in order to acquire data. This data is then used to fit the mapping of the look-up table onto.

Hydraulic Servo System

The spool position of the valve will determine the oil flow into the cylinder. The working principles of the Hydraulic Servo System (HSS) will be further explained in detail in Chapter 3.

Hydraulic Power Unit

The Hydraulic Power Unit (HPU) supplies the hydraulic power that the system needs. The Piston Type Accumulator (PTA) is added to accommodate for any peak flow when the HPU is insufficient. The PTA is an additional oil reservoir pressurized by a set of nitrogen tanks. The PTA can also accommodate for failure of both HPUs by providing enough flow to keep the system operational for 60 seconds.

Control Panel

The system is operated by two operators, hence the two control panels. One is positioned on the transfer deck, whereas the other is placed on the vessel. The operators can control the platform and gangway. The operators have no influence on the motion compensation done by the Stewart platform.

2-2 Ampelmann Safety Management System

As previously stated, the Ampelmann system is designed to be fail-operational. An ASMS is employed to monitor all parts fo the system and accommodate for any faults and failures in the system. The ASMS is independent of the motion control system.

2-2-1 Operational States

The Ampelmann system has four operational states:

- **Safe Mode**

- **Settled State**

- **Neutral State**

- **Engaged State**

When the system pressure is turned on, the system will start in safe mode. The springs in the valves are configured such that the equilibrium of the spool is at -10 % to keep the cylinders retracted. Thus during safe mode the cylinders are not controlled by the motion compensation control loop as pictured in Figure 2-3.

The PLC will perform a pre-starting check. After checking if everything is OK, the system will automatically go from safe mode to settled. In settled mode, the cylinders are still kept at their minimal lengths, however, now they receive the same negative control signal from the motion control loop. The operator on the transfer deck is now able to switch between settled, neutral and engaged as shown in Figure 2-4. When the platform is in neutral state, all cylinders are at half their maximum length. When the system is in engaged state, the actual motion compensation is done.

The operator will be notified of any warnings and alarms that the system gives. All possible failures and faults are classified and connected to one of the alarm levels as given in Table 2-1.

When a code yellow occurs, the operator can continue operation as normal. During a code orange, the operator needs to finish operation within one minute and then go back into settled state. However, during a code red or black, the alarm will be relayed to all crew. The system will automatically go into safe mode as this is an emergency condition. This can be commanded through the PLC (software) or by switching on timed relays (hardware).
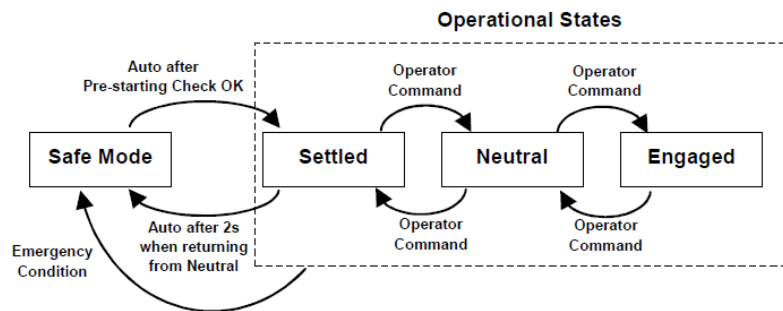
Figure 2-4: Sequence of platform states [1]

Table 2-1: Different levels of alarms for the Ampelmann system

Level	Cause	Action
Code Yellow	Minor Warnings	Continue Operation
Code Orange	Non-critical Failure	Finish Operation in 60 seconds
Code Red	Critical Failure	System shut down through software in 5 seconds
Code Black	Critical Failure	System shut down through hardware in 5 seconds

2-3   Summary

To conclude this chapter, the Ampelmann system already has a safety management system which monitors and accounts for all possible failures. Safety-critical components are redundant in the system to accommodate single component failure. There are still occasions when the system goes into safe mode as result of an emergency condition. This predominately occurs due to double component failures.

Chapter 3

Modelling of the Hydraulic Servo System

In this chapter the focus will be on deriving a mathematical model for the Hydraulic Servo System (HSS) in the Ampelmann system. This mathematical model will be based on first principles. In Section 3-1, the HSS for the Ampelmann system will be introduced. In Section 3-2, the different subsystems of the HSS are discussed which will then be combined into a non-linear and linear mathematical model for the HSS in Section 3-3.

3-1   The Hydraulic Servo System in the Ampelmann System

The motion compensation of the Ampelmann system is accomplished through actuating six hydraulic cylinders, Figure 3-1. The actuator is an asymmetric, two-way operated hydraulic cylinder with a three-stage servo-valve.

Each cylinder is closed-loop controlled, based on calculations from the reference generator and measurements from the sensor equipment on the HSS as briefly explained in Chapter 2.

Hydraulic Cylinder

Figure 3-1: HSS in the Ampelmann system

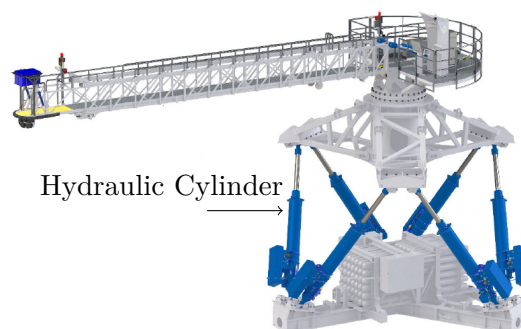The sensor equipment consists of a position transducer and several pressure transducers. The position transducer is of special interest as it is a safety-critical component and will be considered for the Fault Detection (FD) in Chapter 5.

The stroke length of the cylinders is 1.5 meters from its neutral position, where the neutral position of the hexapod is defined as all cylinders at half their maximum heave length. However, they are limited by the workspace of the Ampelmann and will not exceed 1 meter [7]. Due to the fact that the gangway can change position and length, the load mass on the cylinders can be considered variable.

3-2   Subsystems of the Hydraulic Servo System

According to [2], the HSS can be divided into four different subsystems. The four different subsystems are the servo-valve, hydraulic cylinder, power supply and the pipelines in between the first three subsystems. As each HSS is different in its application, there is not a standard model that works equally well for all applications.

Not all subsystems will be of equal importance for the derivation of the final model. This section will mostly treat the servo-valve and the hydraulic cylinder as they have the biggest influence on the dynamics of the piston. The reason for this is that the inflow of oil is controlled by the servo-valve which is the main cause for the movement of the piston.
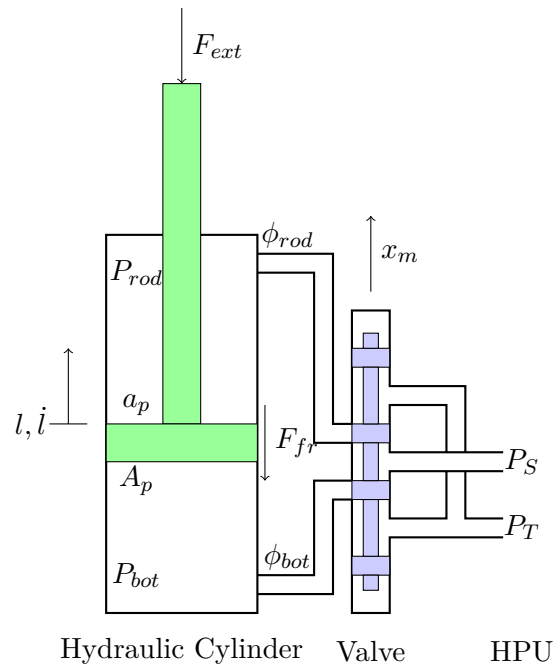
Figure 3-2: Schematic drawing of the Hydraulic cylinder

Figure 3-2 shows a schematic drawing of the hydraulic cylinder and the servo-valve. The hydraulic cylinder consists of the cylinder with two chambers - bottom-side and rod-side - and a piston. The movement of the piston - l, $\dot{l}$ - depends on the pressure difference between the two chambers. The pressures in the chambers -P_{bot}, P_{rod}- are controlled by oil flows - ϕ_{bot},

ϕ_{rod} - from the servo-valve. The spool position - x_m - of the servo-valve determines which port is connected to which chamber. This can be either the high pressure port - P_S - or the low pressure port - P_T from the Hydraulic Power Unit (HPU). The definitions of all variables included in Figure 3-2 are given in Table 3-1.

Table 3-1: Definitions of important variables for the HSS

Variable	Definition	Units
l	Piston position	m
$\dot{l}$	Piston velocity	m/s
P_{bot}	Pressure in bottom chamber	bar
P_{rod}	Pressure in rod-side chamber	bar
A_p	Piston area bottom side	m^2
a_p	Piston area rod side	m^2
ϕ_{bot}	oil flow in and out bottom chamber	m/s^3
ϕ_{rod}	oil flow in and out rod-side chamber	m/s^3
x_m	Spool Position	percentage
P_S	Supply pressure	bar
P_T	Tank/return pressure	bar
F_{fr}	Friction force in cylinder	N
F_{ext}	External force on piston	N

3-2-1   Servo-valve

The servo-valve is a three-stage, four-way operated valve. It consists of a pilot spool and a main spool, Figure 3-3. The input of the servo-valve is generally a voltage or a current. The equations describing the dynamics of the pilot spool and the main spool are given in [2]. For the final model of the cylinder, the main area of interest is that of the piston dynamics, which are mainly influenced by the oil flow in and out of the cylinder. For that reason, the relation between oil flow ϕ and the spool position x_m is of most importance to the final model.
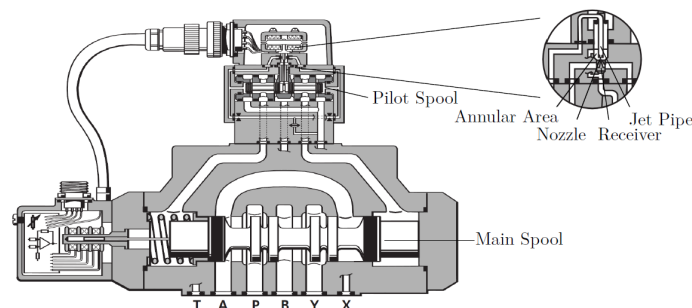

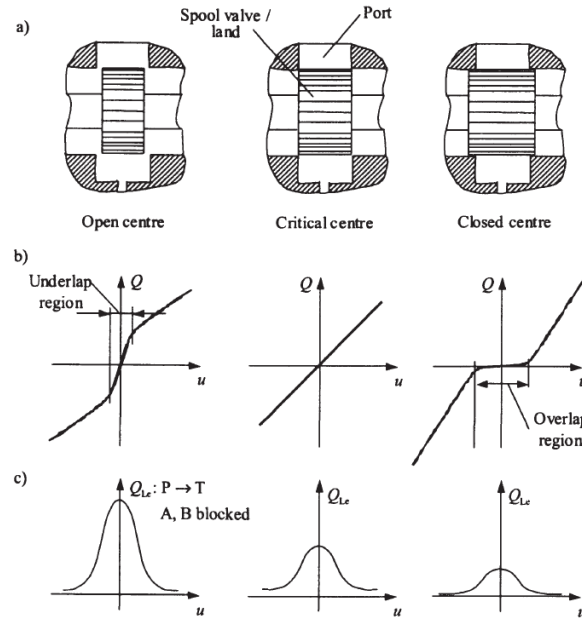**Figure 3-3:** Three-stage Servo-valve

Figure 3-4: (a) Definition of centre types and their corresponding (b) flow-signal graphs and (c) leakage flow curves [2]

Oil Flow

The oil flow is determined by the spool position x_m in the valve. If the valve opens, there will be a turbulent flow from the high pressure port to the low pressure port [3]. The flow has a square-root dependence on this pressure difference. Furthermore, it depends on the type of spool, Figure 3-4.

Figure 3-4 shows that the relation between flow and valve input is non-linear unless it has a critical centre. However, in practice a critically centred spool valve is not ideal because the chance of leakage flows is much higher. Thus to reduce leakage flows, a closed centre spool valve has been designed. However, in that case there is an overlap region which results in a jump when reversing direction of control signal. To reduce this effect a progressive spool has been implemented, Figure 3-5. Nonetheless, the oil flow should be considered as a non-linearity in the system. A non-linear flow function can be identified, such that it can be modelled as a non-linear input.

The oil flow can be given by the following equation:

$$\phi = C_d A_v(x_m) \sqrt{\frac{2(P_1 - P_2)}{\rho}} \tag{3-1}$$

where C_d is the discharge coefficient, $A_v(x_m)$ is the valve area dependent on the spool position, P_1 the pressure at the high pressure port, P_2 the pressure at the low pressure port and ρ the oil density. This relation can describe the oil flowing into either chamber, (3-2) (3-3), depending on the spool position. The function f_{NL} describes the non-linearities of the spool as well as any leakages. The non-linear function can be identified from experimental data.
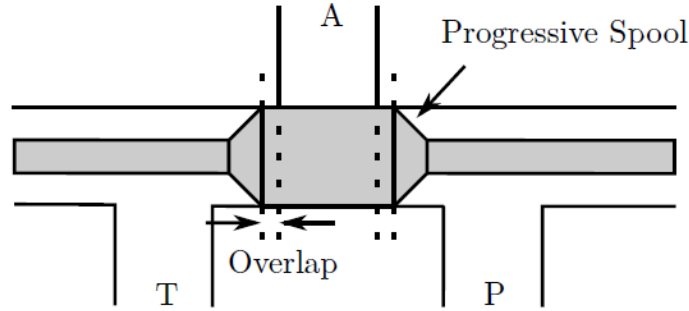
Figure 3-5: A progressive spool [3]

$$\phi_{bot} = \begin{cases} f_{NL}(x_m)\sqrt{P_S - P_{bot}} & \text{if } x_m \geq 0 \\ f_{NL}(x_m)\sqrt{P_{bot} - P_T} & \text{if } x_m < 0 \end{cases} \tag{3-2}$$

$$\phi_{rod} = \begin{cases} f_{NL}(x_m)\sqrt{P_{rod} - P_T} & \text{if } x_m \geq 0 \\ f_{NL}(x_m)\sqrt{P_S - P_{rod}} & \text{if } x_m < 0 \end{cases} \tag{3-3}$$

To reduce the order of the final model, it is useful to describe the oil flow with one single equation. In order to achieve this, the concept of load pressure P_L can be introduced. For an asymmetric actuator, the load pressure is defined as the difference between the pressures in the two chambers but taking into account the difference in piston area [9].

$$P_L = P_{bot} - \alpha \cdot P_{rod} \tag{3-4}$$

where

$$\alpha = \frac{a_p}{A_p} \tag{3-5}$$

This relationship can be used to simplify the oil flow functions into one single equation for the load flow ϕ_L.

$$\phi_L = \frac{\phi_{bot} + \phi_{rod}}{2} \tag{3-6}$$

$$\phi_L = f_{NL}(x_m)\sqrt{P_S - \text{sign}(x_m)P_L} \tag{3-7}$$

This concludes the servo-valve for the final model, in which the oil flow has the most relevance. It can be seen as the input for the hydraulic cylinder.

3-2-2 Hydraulic Cylinder

As the goal of the final model is to model the dynamics of the piston, the dynamics of the hydraulic cylinder are of most interest. The dynamics depend on the pressure dynamics as well as the equations of motion for the piston. The hydraulic cylinder model can be described by a 3rd order state-space model.

The pressure dynamics can be given in terms of load pressure [2, 9]. The oil flow has a direct influence on the way the pressure changes. Thus it can be modelled as the input of the hydraulic cylinder model:

$$\dot{P}_L = -\alpha\dot{x} - \beta P_L + f_{NL}(x_m)\sqrt{P_S - \text{sign}(x_m)P_L} \tag{3-8}$$

The load pressure dynamics depend on a change in volume of the cylinder chambers as defined by the piston velocity, cylinder volume, piston area and the effective bulk modulus. These four factors are incorporated into parameter α. Furthermore, the cylinder volume, piston area, effective bulk modulus and a leakage coefficient are incorporated into parameter β in order to determine the influence of the load pressure on the load pressure dynamics.

The equation of motion for the piston is given by:

$$m\ddot{x} = -kx + A_p P_L - F_{fr}(\dot{x}) \tag{3-9}$$

where m is the load mass and k is the actuator stiffness. The main non-linearities are present in the friction force F_{fr}.

Friction Force

The friction force plays an important role in the dynamics of the hydraulic cylinder piston and depends on the velocity of the piston. The friction force can be described by a combination of static, viscous and Coulomb friction.

$$F_{static} = \begin{cases} sign(F_{ext} \cdot \min(F_{s,max}, F_{ext})) & \dot{x} = 0 \\ 0 & \dot{x} \neq 0 \end{cases} \tag{3-10}$$

$$F_{Coulomb} = \begin{cases} 0 & \dot{x} = 0 \\ sign(\dot{x}) \cdot F_{c0} & \dot{x} \neq 0 \end{cases} \tag{3-11}$$

$$F_{viscous} = \mu_v \cdot \dot{x} \tag{3-12}$$

These equations can be combined into one friction curve which is usually referred to as the Stribeck friction curve, Figure 3-6. With the Stribeck friction curve, the static friction jump is described more realistically. The Stribeck friction curve is given in the following equation:

$$F_{fr} = \mu_v \cdot \dot{x} + sign(\dot{x})(F_{c0} + F_{s0} \cdot e^{(-\frac{|\dot{x}|}{c_s})}) \tag{3-13}$$

where μ_v is the viscous friction coefficient, F_{c0} the parameter for Coulomb friction, F_{s0} the parameter for static friction and c_s is called the Stribeck velocity.

The parameters of the friction function can be identified experimentally. This is done by carrying out constant velocity experiments. However, it should be noted that the cylinder is not attached to a rigid body, i.e. the ship is moving. Thus dynamic forces may be significantly larger than the friction force.
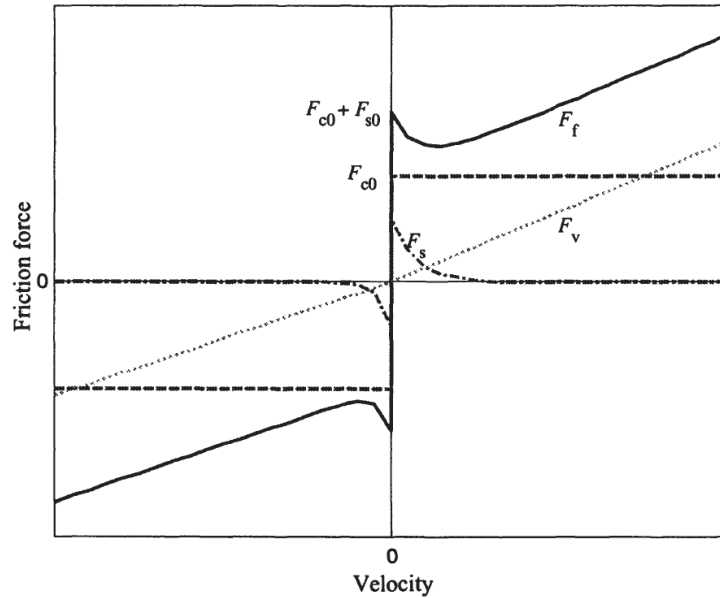
Figure 3-6: Velocity-dependent friction force (Stribeck curve) [2]

3-2-3 Power Supply

The HPU is said to supply a high pressure of 250 bar. However, in practice this is not exactly the case. In Figure 3-7, the supply pressure when the system is in engaged mode is shown. It is evident from the graph that the supply pressure that arrives at the hydraulic cylinder is neither constant nor 250 bar.

3-2-4 Pipelines

All subsystems are connected by pipelines. Pipelines can be modelled as an inefficient volume of the respective cylinder chamber. However, for the Ampelmann HSS, the servo-valve is
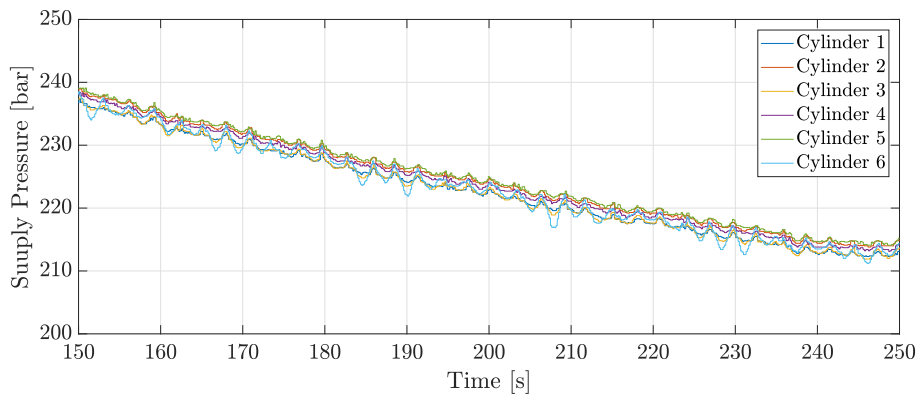
Figure 3-7: Supply pressure while in operation.

placed directly onto the cylinder, thus the effect is negligible.

3-3   Mathematical Model

By integrating all the knowledge introduced in the previous sections, a non-linear model can
be derived. Furthermore, additional assumptions are made which will result in a linear model
that can be identified from experimental data. For both the non-linear and linear model, the
same states are assumed:

$$
x = \begin{bmatrix} l \\ \dot{l} \\ P_L \end{bmatrix}
\tag{3-14}
$$

Both models will be represented in observer canonical form.

3-3-1   Non-linear Representation

For the non-linear model, the friction force is modelled as the Stribeck friction curve given in
(3-13). Furthermore, the non-linear function which is found from experimental data is defined
as the non-linear input of the model. Combining (3-8) and (3-9) into one model, it follows
that:

$$
\dot{x}(t) = f(x(t), u(t)) = \begin{bmatrix} x_2(t) \\ -\frac{k}{m} x_1(t) - \frac{1}{m} F_{fr}(x_2(t)) + \frac{A_p}{m} x_3(t) \\ -\alpha x_2(t) - \beta x_3(t) + f_{NL}(u(t))\sqrt{P_S - sgn(u(t))x_3(t)} \end{bmatrix}
\tag{3-15}
$$

$$
y(t) = \begin{bmatrix} 1 & 0 & 0 \\ 0 & 1 & 0 \end{bmatrix} \cdot x(t)
\tag{3-16}
$$

Non-linear Flow Function

The function $f_{NL}(x_m)$ describes the non-linearities of the servo-valve due to shape of the
spool and leakage flows. The function has been approximated by using a singleton fuzzy
model. In Figure 3-8 it can be observed that the flow is different for each cylinder, especially
for positive valve openings. Hence the function needs to be identified individually for each
cylinder.

The non-linear flow function is approximated using a singleton fuzzy model with 20 mem-
bership functions. The choice for using a singleton fuzzy model is motivated by [4] where it
has been done for the smaller Ampelmann A-type. The flow ϕ is approximated by using the
following relation:

$$
\phi = \begin{cases} A_p \cdot \dot{x} & \text{if } x_m > 0 \\ \alpha A_p \cdot \dot{x} & \text{if } x_m < 0 \end{cases}
\tag{3-17}
$$
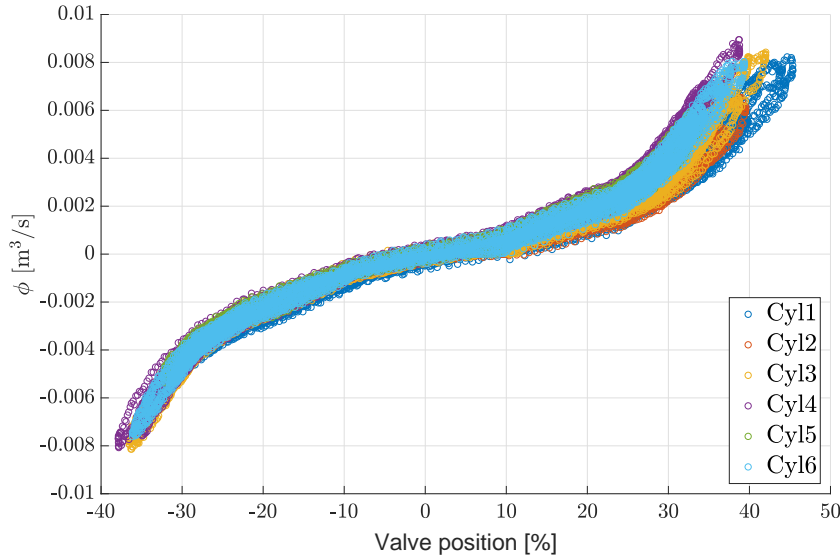
Figure 3-8: Inflow cylinder with respect to the valve position for all six cylinders

The function can then be approximated by:

$$f_{NL}(x_m) = \frac{\phi}{\sqrt{P_S - \text{sign}(x_m)P_L}} \tag{3-18}$$

The approximation of the non-linear flow function for Cylinder 1 is presented in Figure 3-9.

Friction Force

It is presumed that the friction force is equal to the external force minus the load force:

$$F_{fr} = F_{ext} - A_p P_L \tag{3-19}$$

However, when plotting the expected friction force versus the velocity from experimental data there is no apparent relation between the calculated force and velocity, Figure 3-10.

This could be due to the fact that the cylinder is not attached to a rigid body. Thus it is difficult to identify the friction due to high dynamic forces in the system, since the cylinder is attached to the ship and the platform which are both not rigid.

To obtain data for a friction curve compared to the one presented in Figure 3-6, a constant velocity experiment can be carried out. However, this is not considered in this thesis. Because the non-linearity in the friction force is not easily identifiable, the next section will explore the option of identifying a linear model.

Figure 3-9: Approximation of the non-linear flow model using Singleton Fuzzy model

3-3-2   Linear Representation

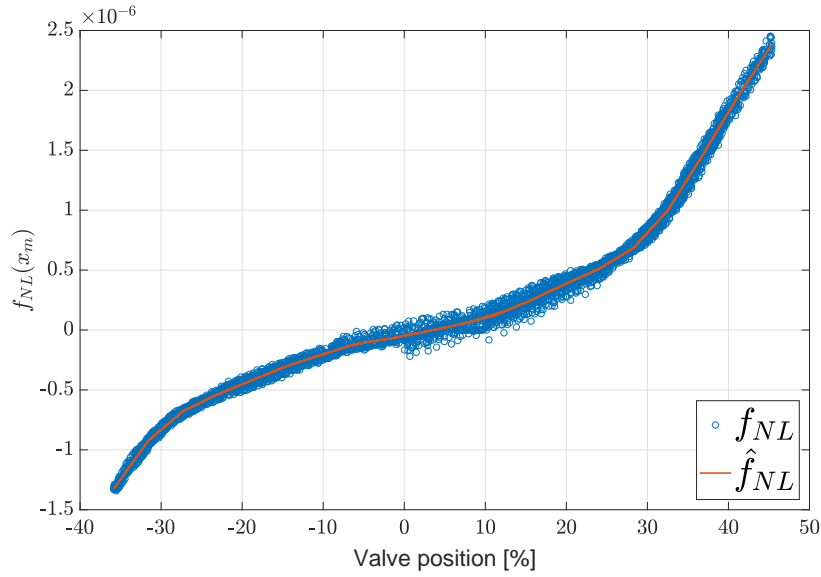For the linear model, additional assumptions have been formulated. When looking at the control scheme, Figure 3-11, it can be observed that the control signal from the controller is sent to a look-up table which transforms the control signal to a spool position. For the non-linear model, the spool position was considered as the input. The non-linear function f_{NL} is similar to the look-up table. When considering a model of everything inside the dashed line in Figure 3-11, the non-linearity of the spool can be taken out.

The input of the linear model can be considered the same as the control input $\dot{i}_{ctrl}$. The next assumption for the linear model is that only viscous friction occurs in the system. That reduces the friction force to:

$$F_{fr} = \mu_v \cdot x_2 \tag{3-20}$$

Taking all of this into account, it results in the following linear state-space model:

$$\dot{x}(t) = Ax(t) + Bu(t) = \begin{bmatrix} 0 & 1 & 0 \\ -\frac{k}{m} & \mu_v & \frac{A_p}{m} \\ 0 & -\alpha & -\beta \end{bmatrix} x(t) + \begin{bmatrix} 0 \\ \gamma_1 \\ \gamma_2 \end{bmatrix} u(t) \tag{3-21}$$

$$y(t) = \begin{bmatrix} 1 & 0 & 0 \\ 0 & 1 & 0 \end{bmatrix} \cdot x(t) \tag{3-22}$$

It is assumed that the control input influences both the pressure dynamics and the piston dynamics. The exact influence is not determined yet but γ_1 and γ_2 can be identified from experimental data.
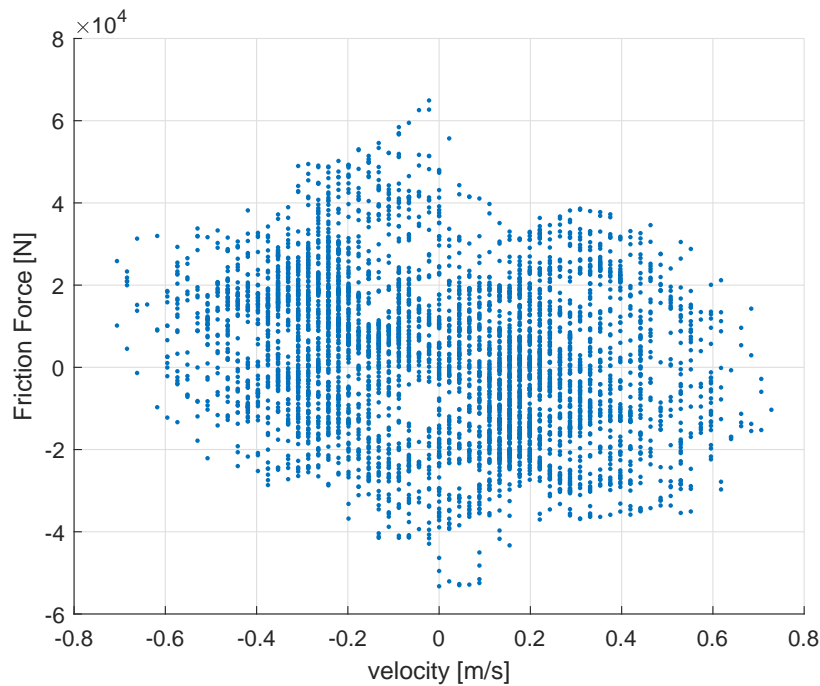
Figure 3-10: Experimental data for friction identification
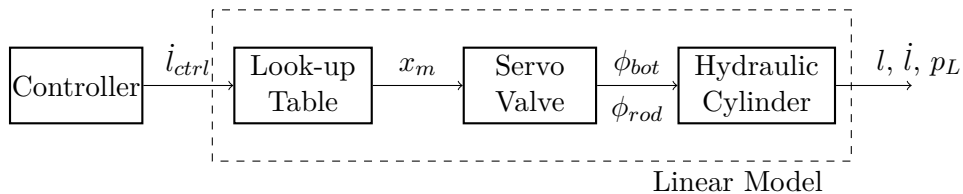
Figure 3-11: Block scheme for linear model

3-4 Summary

In this chapter, a model based on first principles of the HSS has been derived. However, due to the number of unknown and uncertain parameters, this model alone is not sufficient to be used for fault detection. It does, however, give some insight into the dynamics of the HSS. The main non-linearities in the system are the pressure dependencies of the oil flow and the friction force. As the friction force cannot be identified with the current data, a non-linear representation is undesirable. For that reason, a linear model will be identified in Chapter 4.

Chapter 4

System Identification

In this chapter, the identification of the model for the Hydraulic Servo System (HSS) will be discussed, which is based on the mathematical model from Chapter 3. The model is a grey-box model whose the parameters are identified by solving a linear least squares problem. In Section 4-1 the data that is used for identification and validation of the model is studied. In Section 4-2, the identification of the grey-box model using linear least squares is analysed. Finally, the validation of the identified model is explored in Section 4-3.

4-1 Identification Data

For the identification and validation of the model, data has been gathered during offshore operation of the E-08. The data has been logged with a sampling frequency of 50 Hz. From Chapter 3 it follows that the relevant signals for the identification procedure are the control speed - $\dot{l}_{ctrl}$ -, the cylinder position - l -, the cylinder speed - $\dot{l}$ - and the load pressure - p_L-, Figure 4-1.

The velocity signal, Figure 4-1c, and the load pressure signal, Figure 4-1d, are noisy. These signals will be pre-filtered before being used for identification. The signals are filtered by applying a moving average filter to smooth the signal, Figure 4-2. The moving average filter will ensure that there is no phase-shift when filtering the data.

The dataset can be split up into six different sets, one set per cylinder. Hence, dataset 1 will correspond to Cylinder 1, dataset 2 to Cylinder 2 and so forth. It should be noted that the data shown in Figure 4-1 and Figure 4-2 is the data that correspond with Cylinder 1.

The validation of the model is done with a different dataset. For the validation, the velocity signal is smoothed. Load pressure is only used for identifying parameters and is thus not used for the validation.
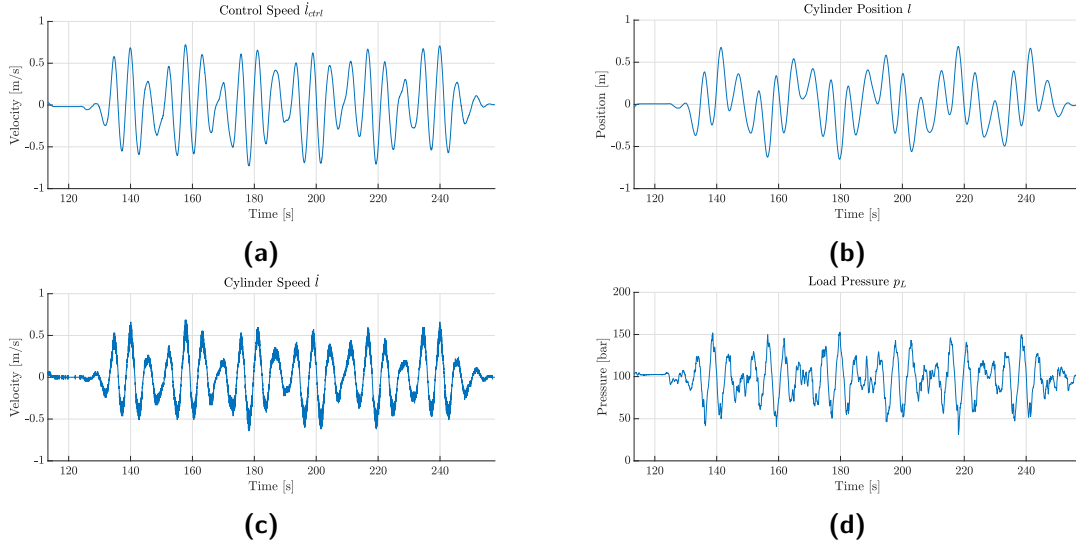
Figure 4-1: Identification Data
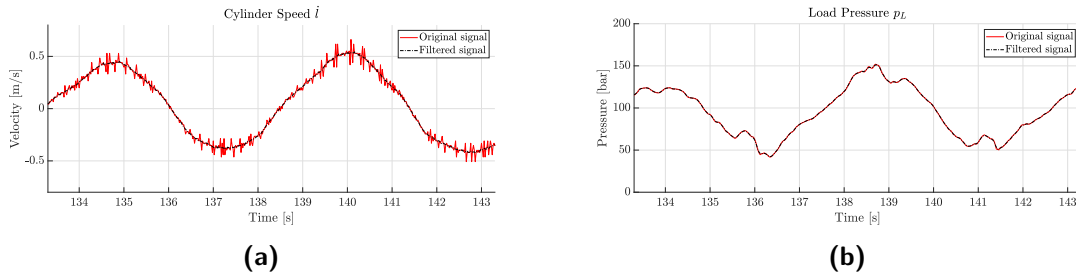
Figure 4-2: Smoothed signals

4-2   Grey-box Identification

The Least Squares (LS) approach is used for identifying the model. The assumption made for using this approach is that the model can be described by a linear-in-the-parameters model. For this, the discretized linear state-space representation is used which follows from Section 3-3-2. The identified model is a dark grey-box model as there cannot be any conclusions made about the values of the identified variables with respect to the real-life variables explained in Chapter 3. However, there are some zeros, and T_s is defined beforehand. Therefore, the model that will be identified will be of the following form:

$$x(k+1) = \begin{bmatrix} 1 & Ts & 0 \\ \theta_1 & 1+\theta_2 & \theta_3 \\ 0 & \theta_4 & 1+\theta_5 \end{bmatrix} x(k) + \begin{bmatrix} 0 \\ \gamma_1 \\ \gamma_2 \end{bmatrix} u(k) \tag{4-1}$$

Thus it follows that there are seven parameters that need to be identified. The model will be rewritten as a linear-in-the-parameters form:

$$y = \phi^T \theta \tag{4-2}$$

$$x(k+1) = (A+I)x(k) + Bu(k) \tag{4-3}$$

$$x(k+1) - x(k) = Ax(k) + B(k) \tag{4-4}$$

Hence $y = x_i(k+1) - x_i(k)$ for $i = 2, 3$ and $\phi = \begin{bmatrix} x_1(k) & x_2(k) & x_3(k) & u(k) \end{bmatrix}$ lead to θ which contains the unknown parameters. There are no assumptions made on process or measurement noise. For that reason, the LS approach will give a biased estimate of the parameters. The LS approach will now find a parameter estimate $\hat{\theta}$ using:

$$\hat{\theta} = (\phi^T \phi)^{-1} \phi^T y \tag{4-5}$$

Which gives the LS estimate that minimizes the quadratic cost function of the prediction error:

$$V(\hat{\theta}) = \frac{1}{N} \sum_{k=1}^{N} (y(k) - \phi^T(k)\hat{\theta})^2 \tag{4-6}$$

The LS problem will be solved for two separate linear regression models: one for x_2 and one for x_3.

$$X_2(k+1) - X_2(k) = \begin{bmatrix} X_1(k) & X_2(k) & X_3(k) & U(k) \end{bmatrix} \begin{bmatrix} \theta_1 \\ \theta_2 \\ \theta_3 \\ \gamma_1 \end{bmatrix} \tag{4-7}$$

$$X_3(k+1) - X_3(k) = \begin{bmatrix} X_2(k) & X_3(k) & U(k) \end{bmatrix} \begin{bmatrix} \theta_4 \\ \theta_5 \\ \gamma_2 \end{bmatrix} \tag{4-8}$$

where X_1, X_2, X_3 and U are the data vectors containing $N - 1$ data points that have been gathered during operation.

As mentioned in Section 4-1, the data that has been gathered can be split up into six sets. One set will be used for identification whereas the other five can be utilized to cross validate the identified model across the other cylinders. There are, however, more sets available from other operations which can also be used for validation. Hence the identified model can be cross-validated using six different sets. From Figure 4-3 it can be seen that not all sets are equally capable in identifying the model. Datasets 2, 4, 5 and 6 can be discarded as identification sets as the model identified with these sets has a low Variance Accounted For (VAF) score when validating with a validation set for Cylinder 3. The models identified using datasets 1 and 3 both perform well, however, when cross-validated, the model identified with dataset 3 performs slightly better. It would be expected that a model identified and validated on its own set would have a higher VAF value than any other validation with a random set. However, when observing Figure 4-3 this is not the case. This will be explored in more detail in the next paragraph.
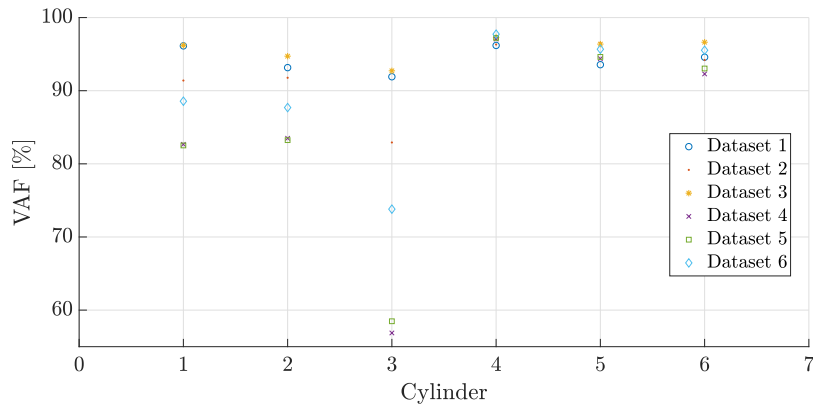
Figure 4-3: Variance Accounted For per identified model validated with all six sets

The model identified with data from Cylinder 3 has the best overall performance when validating the model. It is known that the demand of performance is not equal on all cylinders during operation. The external force exerted on all cylinders is not equally divided as the masses of the platform, gangway and personnel are not equally distributed. Especially the position of the gangway has an influence on the unequal distribution of mass. The model should be able to generalize this variation. The varying mass distribution will influence the pressure in the cylinder chambers and thus influence the load pressure.

In Figure 4-4 it can be observed that there are large differences between the load pressure in the cylinders. When the system is in engaged mode and compensating for the vessel motions, this is normal behaviour. However, the difference shown in the first half of the graph is when the system is in neutral state, meaning all cylinders are at half their maximum length. If the mass would be equally distributed, the load pressures should not differ much here. However, due to the position for the gangway the mass is unevenly distributed.
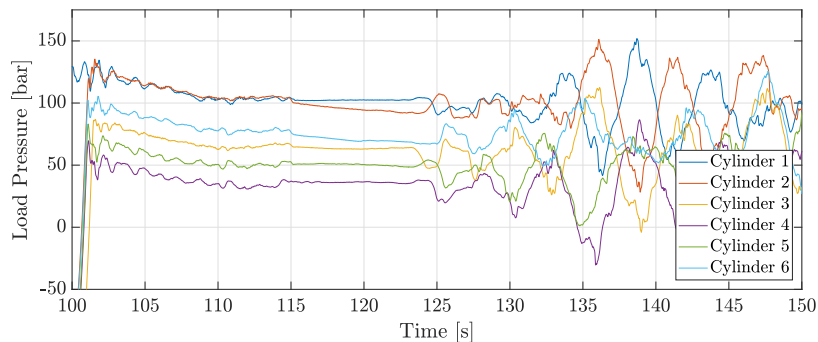
Figure 4-4: Arbitrary section of data of the load pressure for each Cylinder

When looking at the dataset from Cylinder 3, it can be observed that, while in neutral state, the load pressure comes closest to the average load pressure of all cylinders. This could be a reason that the model identified using Dataset 3 works equally well for all the cylinders.

The parameters estimated using dataset 3 are given in Table 4-1. The estimated model will be validated in the next section.

Table 4-1: Estimated parameters

Parameter	Value
θ_1	-0.0101
θ_2	-0.1231
θ_3	$-1.6891 * 10^{-5}$
θ_4	-10.7104
θ_5	-0.0023
γ_1	0.0926
γ_2	6.5427

4-3   Model Validation

The model identified using the linear least squares approach needs to be validated in order to ensure that the obtained model is a good model. The previous section already briefly touched upon the subject of validation when cross-validating the models using a different dataset. In the previous section, the model was cross-validated using a validation dataset across all six cylinders. The VAF values were all above 90%, which is satisfactory. In Figure 4-5 and Figure 4-6 the simulated response is presented for Cylinder 1 using the identified model.

Figure 4-5: Simulated Cylinder position for Cylinder 1
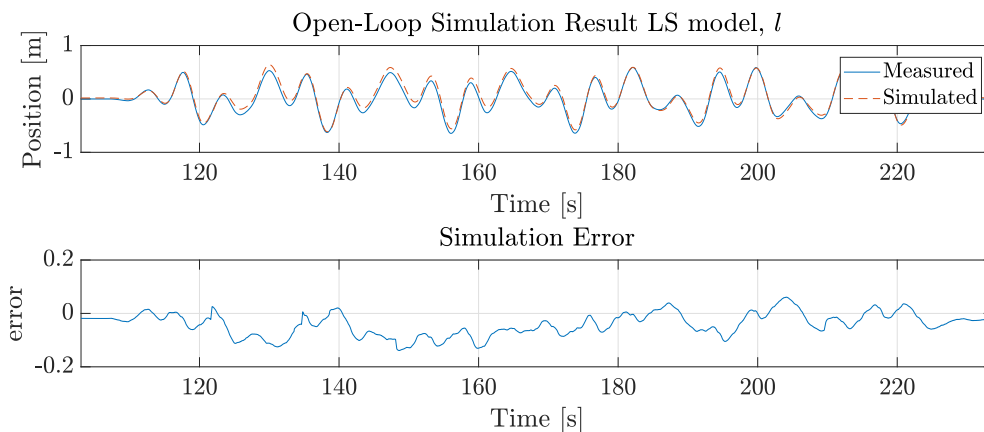
Simulation errors of about 15 cm and 7.5 cm/s still occur for the position and velocity respectively. However, this can be accounted for by using an observer or Kalman filter, Figure 4-7. The spikes that are observed on the error are due to missing data points. Assuming the filter will get the measurements from the transducer when running, the Kalman filter can be used to accurately estimate the position.

The model can be further validated using residual tests [10]. It should be noted that the identification is done using data from a closed loop experiment i.e. the input for the next step depends on the output of the previous step.
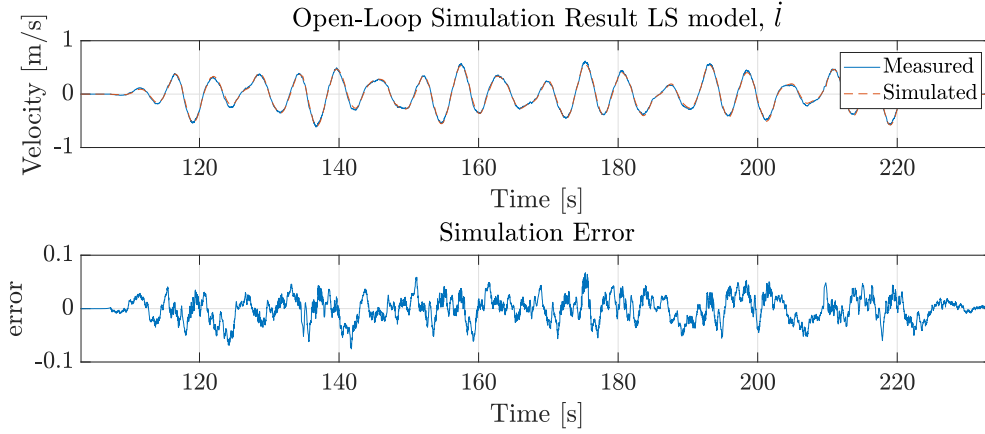
Figure 4-6: Simulated Cylinder velocity for Cylinder 1
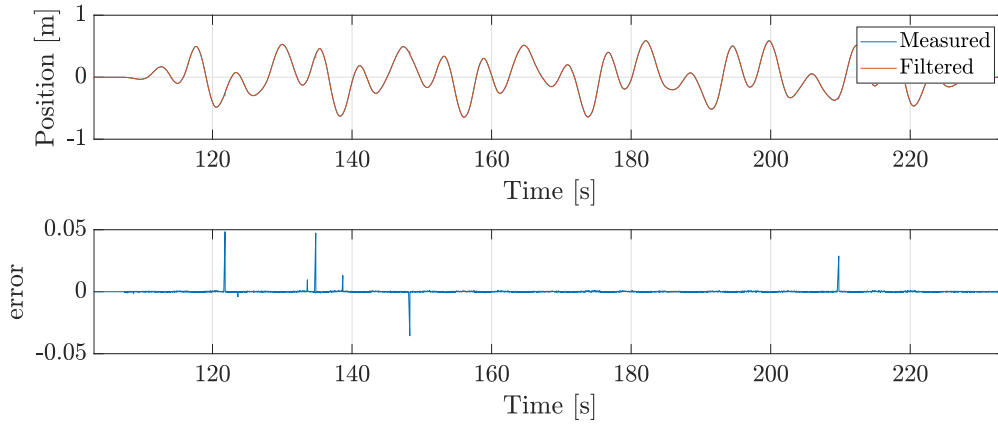
Figure 4-7: Simulated Cylinder position with a Kalman filter

Residual tests inspect whether the error sequence can be considered a zero-mean white noise sequence and whether the error sequence is statistically independent from the input. This error sequence follows from the prediction error from the Kalman Filter equations:

$$\hat{x}(k+1, \hat{\theta}) = \left(A(\hat{\theta}) - K(\hat{\theta})C(\hat{\theta}) \right) \hat{x}(k, \hat{\theta}) + \left(B(\hat{\theta}) - K(\hat{\theta})D(\hat{\theta}) \right) u(k) + K(\hat{\theta})y(k) \qquad (4\text{-}9)$$

$$\hat{\epsilon}(k, \hat{\theta}) = y(k) - C(\hat{\theta})\hat{x}(k, \hat{\theta}) - D(\hat{\theta})u(k) \qquad (4\text{-}10)$$

The auto-correlation of the error sequence should approximate a unit pulse if the error sequence is a zero-mean white noise sequence, whereas the cross-correlation of the error sequence and input should be approximately zero if they are statistically independent. The residual auto-correlation for the position does indeed approximate a unit pulse, Figure 4-9a, which means that the residuals of the position estimation are white, i.e. uncorrelated. The residual auto-correlation for the velocity estimates does not approximate a unit pulse, Figure 4-9b. The error sequence cannot be considered white, which is in accordance with the error sequence
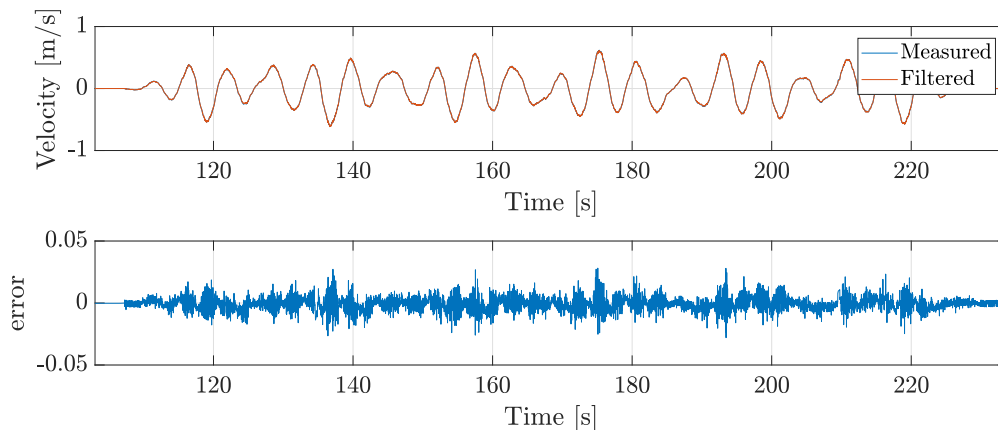
Figure 4-8: Simulated Cylinder velocity with a Kalman filter

as shown in Figure 4-8. However, the model will only be used to estimate the position of the Cylinder thus the result of the residual test for the velocity can be neglected.

The cross-correlation plots, Figure 4-9c and Figure 4-9d, show the correlation between the input signal and the residuals. This tests the independence of the residuals with the past inputs. As mentioned earlier in this section, the identification is done with data from a closed-loop experiment. From the fact that it is closed-loop, it follows that there is a dependence on past inputs as there is a form of feedback. Thus the model cannot pass the auto-correlation test [10].

When observing the auto-correlation test it can be concluded that the model is good for estimating the position, which is what it will be used for. However, it is not as good for estimating the velocity as the auto-correlation test is not passed. The cross-correlation test is not passed which can be explained by the fact that the data is from a closed-loop experiment. Thus the output is dependent on past inputs.
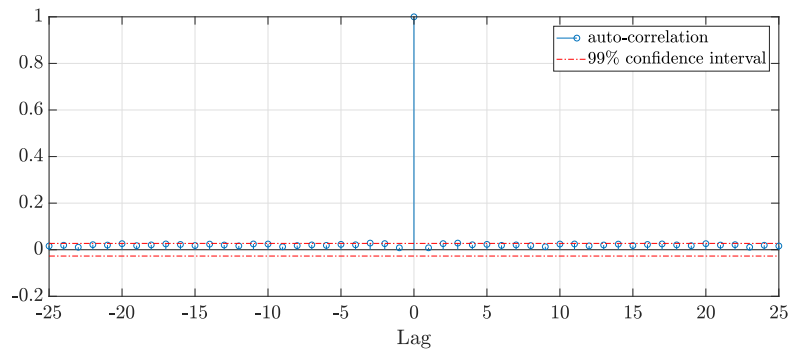
(a) Auto-correlation for the residual of the first output l
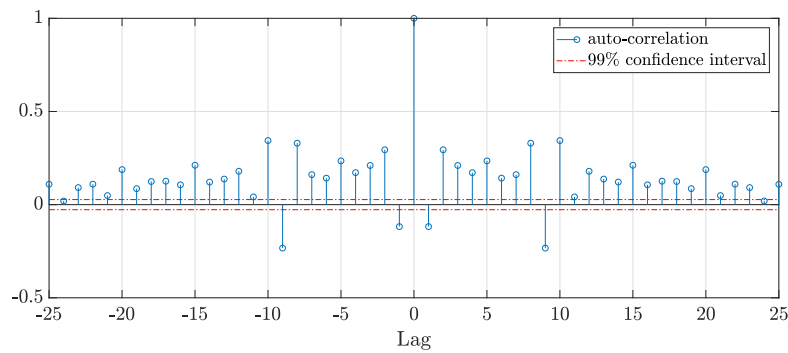
(b) Auto-correlation for the residual of the second output $\dot{l}$
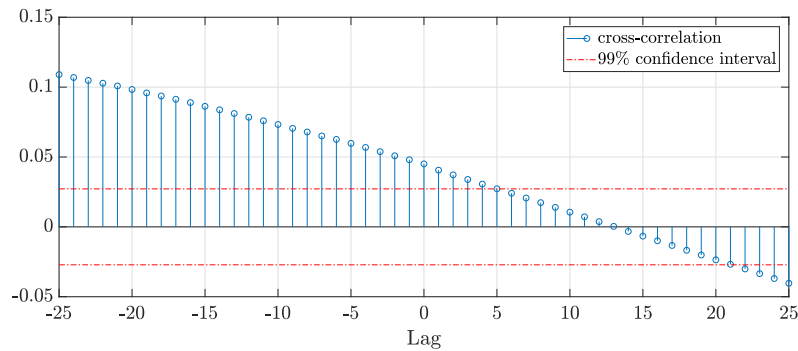
(c) Cross-correlation for the residual of the first output l and the input $\dot{l}_{ctrl}$
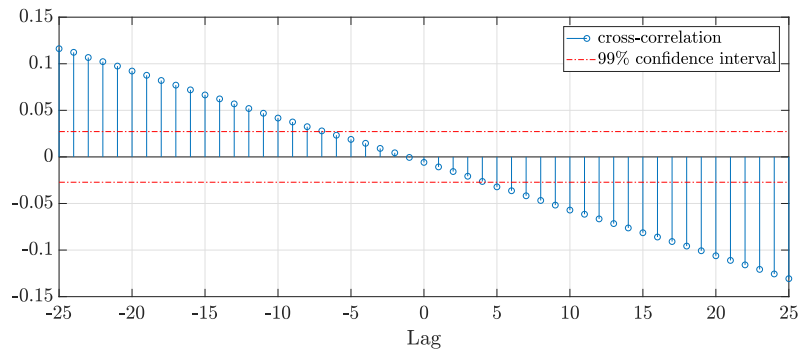
(d) Cross-correlation for the residual of the second output $\dot{l}$ and the input $\dot{l}_{ctrl}$

Figure 4-9: Auto- and Cross-correlations for the residuals

4-4   Summary

In summary, the data that has been used for identification and validation of the model was gathered during offshore operation of the Ampelmann E-08. The velocity and pressure signal are noisy and therefore pre-filtered before further use. A linear model is identified by solving the linear least squares problem. As it is a dark grey-box model, nothing can be said about the values of the found parameters. The identified model is validated using residual tests. From the residual tests it follows that a good model is obtained for the position estimation as the residuals can be considered uncorrelated and white. Due to the fact that the data was obtained from a closed-loop experiment, the cross-correlation test cannot be checked. The residuals will be dependent on past inputs as there is a feedback loop in the system.

Fault Detection

In this chapter a model-based Fault Detection (FD) Architecture for the position transducer in the hydraulic cylinders will be presented. The FD scheme consists of a bank of Fault Detection Estimators (FDEs). Both abrupt changes as well as slowly developing changes in the sensor can be detected with the bank of FDEs. The method used is a model-based estimation method. In the first section, different fault types are considered and explained. In Section 5-2 the sensor data that comes from the position transducer will be studied. In Section 5-3 the model-based fault detection and residual generation principles are explained. The generated residuals are evaluated in Sections 5-4 and 5-5.

5-1   Faults

The literature defines a fault as *a change in a component such that the operation or performance of said component changes in an undesired way* [5]. They can occur within any part of a system such as the actuators, sensors or the plant itself. In this thesis, a distinction is made between fault and failure. A failure describes the inability of a system or component to accomplish its function. It should be noted that not all literature distinguishes this.

Throughout this chapter, three different types of faults will be referred to, Table 5-1. The faults considered are all additive sensor faults. It is assumed that the fault only influences the output from the sensor. Even though the input of the model depends on feedback from the sensor, this effect is not considered.

Table 5-1: Different fault types

	Fault Type
Type I	Abrupt changes
Type II	Increased noise
Type III	Incipient

Abrupt changes can be modelled with a step-like time profile [11]:

$$\beta(k - k_0) = \begin{cases} 0 & \text{if } k < k_0 \\ 1 & \text{if } k \geq k_0 \end{cases} \tag{5-1}$$

Incipient faults are characterized by an exponential-like time-profile:

$$\beta(k - k_0) = \begin{cases} 0 & \text{if } k < k_0 \\ 1 - (1 + b)^{-(k - k_0)} & \text{if } k \geq k_0 \end{cases} \tag{5-2}$$

where k_0 is the unknown index of the fault occurrence time, $b \leq 1$ is the unknown fault-evolution rate. In Figure 5-1 a few examples of said time-profiles are shown. They determine how a fault will develop over time.
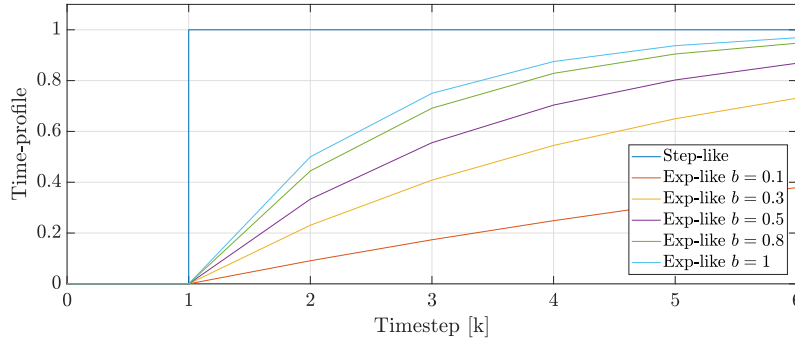
Figure 5-1: Different fault time-profiles

These time-profiles are multiplied with a fault-vector $\phi(y(k), u(k))$ which represents the deviation on the state equation due to the fault [12].

All faults occur in the position transducer and will thus affect the measured values. *A broken wire*, or a value *out of range* is already accounted for in the system thus the focus will lie on those faults that will fall in the category *difference too big*.

5-2   Sensor Data

The Programmable Logic Controller (PLC) receives the measurements from the position transducer as integers which range from 1 to 27648. The PLC will transform these integers to the corresponding lengths in meters.

$$y_m = \frac{y_{int}}{27648} \cdot 3 - 1.5 \tag{5-3}$$

The range of the cylinder in meters is between -1.5 and 1.5, where -1.5 meters is the retracted state and when the cylinder is at 0 meters, it is in neutral state.

The system has a hardware redundancy and thus gets measurements from two position transducers: the main one, C1, and the redundant one, C2. The allowable tolerance before the

system gives a *difference too big* is 5 centimetres. The system will run on the measurements from C1 and will only switch to C2 when C1 is identified as faulty. Thus C2 is primarily used for checking C1.

5-3 Model-based Fault Detection

This thesis focusses on an observer-based approach for fault detection. The model as identified in Chapter 4 is used. This leads to the following equations when there is no fault occurring:

$$\hat{x}_{\text{healthy}}(k+1) = A\hat{x}(k) + Bu(k) + L(y(k) - \hat{y}(k)) \tag{5-4}$$

$$\hat{y}_{\text{healthy}}(k) = C\hat{x}(k) \tag{5-5}$$

An optimal observer gain L is found by computing the optimal gain through the Linear Quadratic Regulator (LQR) design. The optimal gain minimizes the following quadratic cost function:

$$J = x_N^T Q x_N + \sum_{k=0}^{N-1} (x_k^T Q x_k + y_k^T R y_k + 2x_k^T N u_k) \tag{5-6}$$

The matrices Q and R are tuned by hand to find an observer gain for which the residual in the fault-free case is as small as possible.

The fault as defined in Section 5-1 is additive to the sensor output. Thus the observer equations when the fault has occurred will be as follows:

$$\hat{x}_{\text{faulty}}(k+1) = A\hat{x}(k) + Bu(k) + L(y(k) + \beta(k-k_0)\phi(y(k), u(k)) - \hat{y}(k)) \tag{5-7}$$

$$\hat{y}_{\text{faulty}}(k) = C\hat{x}(k) \tag{5-8}$$

The estimates and measurements are used to generate a residual. The residual will be evaluated in order to make a decision about the health of the sensor.

$$r(k) = |y(k) - \hat{y}(k)| \tag{5-9}$$

where in the healthy state,

$$r(k) = |y(k) - \hat{y}_{\text{healthy}}(k)| < \delta \tag{5-10}$$

and after a fault has occurred,

$$r(k) = |y(k) - \hat{y}_{\text{faulty}}(k)| > \delta \tag{5-11}$$

where δ is a pre-defined static threshold. This threshold should be defined such that it will improve the detection before a *difference too big* alarm is given.
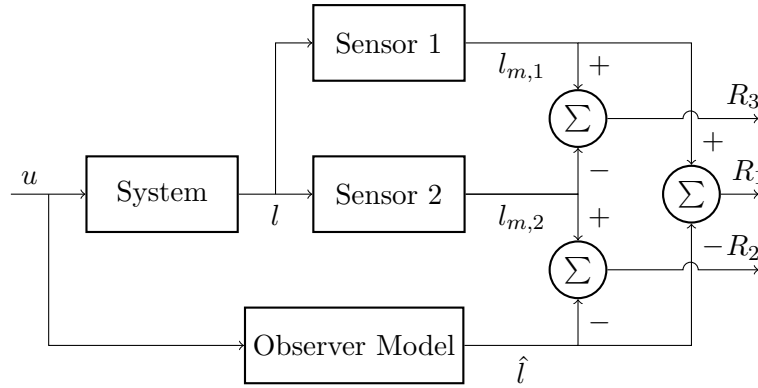
Figure 5-2: Obtaining the residuals

5-3-1   Residual Generation

Three different residuals can be defined based on two position transducers and an observer model, Figure 5-2.

$$R_1 = |y_{\text{C}1} - \hat{y}_{\text{C}1}| \tag{5-12}$$

$$R_2 = |y_{\text{C}2} - \hat{y}_{\text{C}2}| \tag{5-13}$$

$$R_3 = y_{\text{C}1} - y_{\text{C}2} \tag{5-14}$$

The residuals R_1 and R_2 are obtained in a similar manner. Thus only R_1 is discussed as it is assumed that the method for obtaining the results for R_2 is the same. Obtaining residual R_3 is done differently and the reason for this will be discussed in Section 5-5.

The model that was obtained in Chapter 4 is used in combination with an observer gain L to obtain an estimate of the position of the cylinder.

The additive fault will result in a deviation which is not immediately accounted for by the observer. Thus a spike in the residual is expected. When this peak exceeds a pre-defined threshold, the system can give an alarm and switch to the redundant sensor.

In the next few sections, different residuals will be generated and analysed based on the individual fault types. From those results a threshold will be defined. Finally, all estimators that generate residuals will lead to a fault detection architecture that will generate and evaluate these residuals.

5-4   Evaluation of the Residuals for R_1 and R_2

To make a decision about the health of the sensor the residuals are evaluated. Firstly, the fault-free case is considered, Figure 5-3. Then the different fault types discussed in Section 5-1 are evaluated.
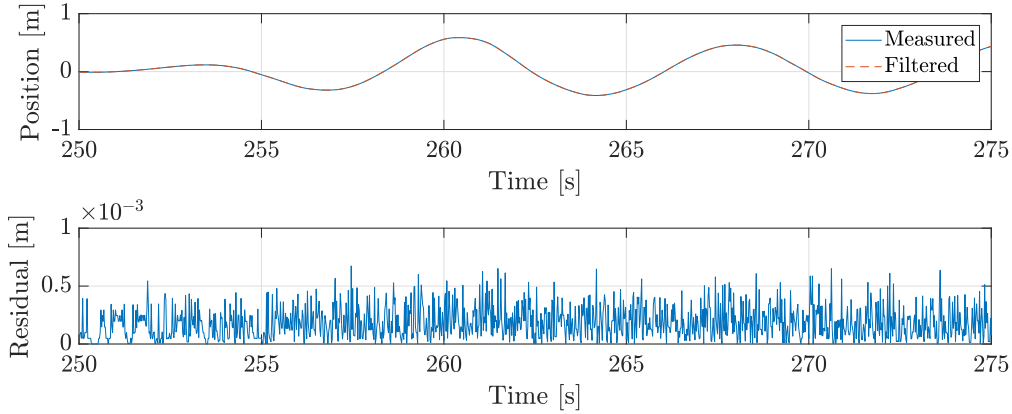
Figure 5-3: Residual for fault-free case.

5-4-1 Fault-free Case

Figure 5-3 shows an arbitrary section of data when the system is in engaged mode. The residual that is generated can be considered small as it stays well below $1 \cdot 10^{-3}$ meters. A lower threshold is defined at $\delta_l = 7.5 \cdot 10^{-4}$ m and an upper threshold at $\delta_h = 1 \cdot 10^{-3}$ m. These thresholds will be used for evaluating R_1 and R_2 for all three fault types.

5-4-2 Fault Type I

Fault type I is modelled as a block signal added to the measurement signal. Different sizes have been considered, ranging from 0.05 m to 0.001 m. These values have been chosen because the current threshold before a *difference too big* happens is 0.05 m while, 0.001 m corresponds to the upper threshold defined in the previous section. Six different sizes are considered, which can be found in (5-15).

$$\phi = \begin{bmatrix} 0.001 \\ 0.0025 \\ 0.005 \\ 0.01 \\ 0.025 \\ 0.05 \end{bmatrix} m \tag{5-15}$$

The fault that will be added over time is shown in Figure 5-4. After the addition of each size, the fault is reduced to zero again. This results in the residual generating a peak for a negative additive fault. Thus it can be shown that these are also detectable.

The results are shown in Figure 5-5. The upper figure shows the signal from the position transducer under normal conditions, with the added fault profile and the estimated signal from the observer. In this figure it is not immediately evident that there are faults present, especially when considering that the fault-free signal would not be available when a fault is present. However, when inspecting the residual plot, a statement can be made about the
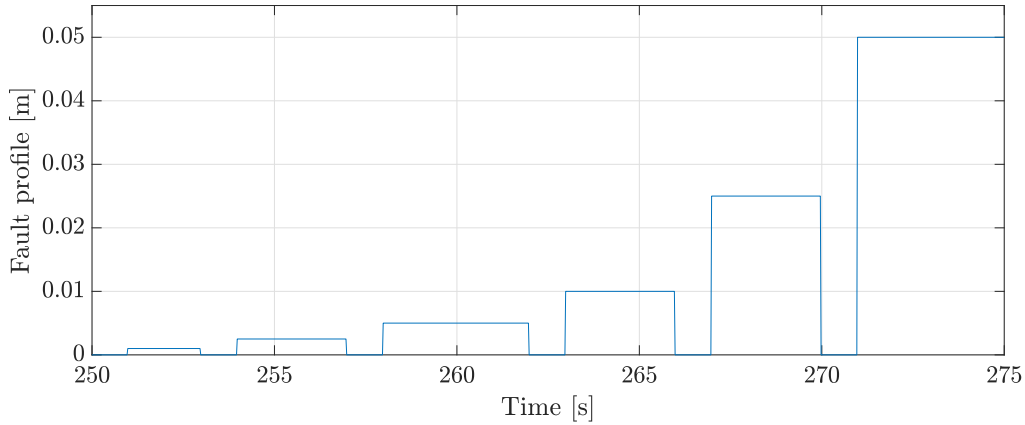
Figure 5-4: Additive Step-like fault profile

added faults. Whenever the signal deviates from the norm, a peak appears in the residual plot. This peak exceeds the thresholds, the dashed red line, as previously defined for all cases except the smallest one of 0.001 m.
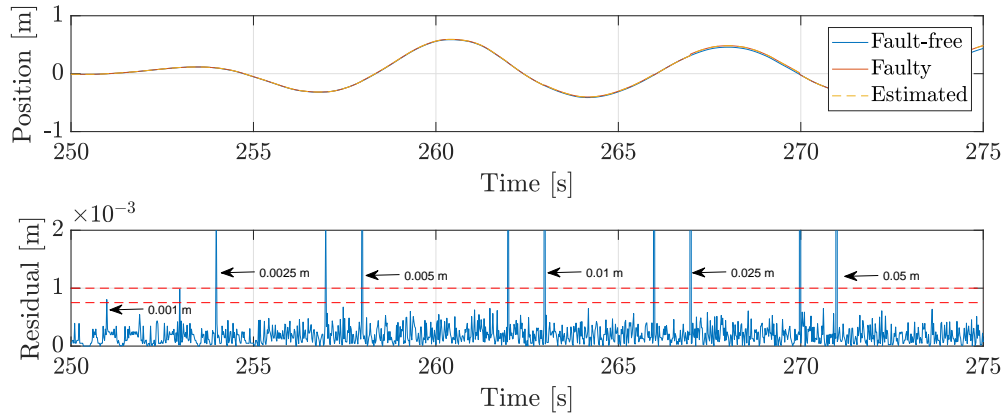
Figure 5-5: Residual for fault type I

So further inspection is executed on fault sizes between 0.001 m and 0.0025 m, Figure 5-6.

$$\phi = \begin{bmatrix} 0.001 \\ 0.00125 \\ 0.0015 \\ 0.00175 \\ 0.002 \\ 0.0025 \end{bmatrix} m \tag{5-16}$$

In the upper plot in Figure 5-7, no evident changes are seen as the added faults are small. When inspecting the residuals, again peaks are identified for all faults larger than 0.001 m.

This means that detection is possible for additive faults as small as 0.00125 m. While looking
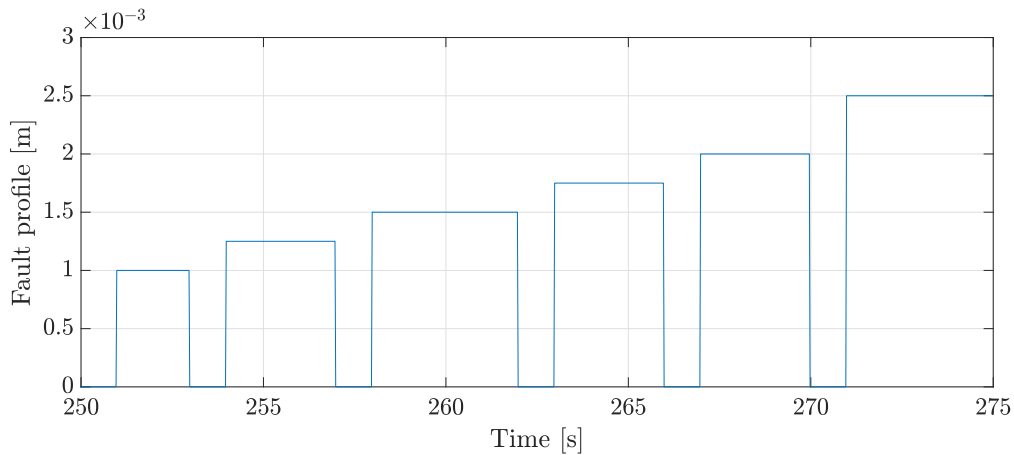
Figure 5-6: Additive Step-like fault profile
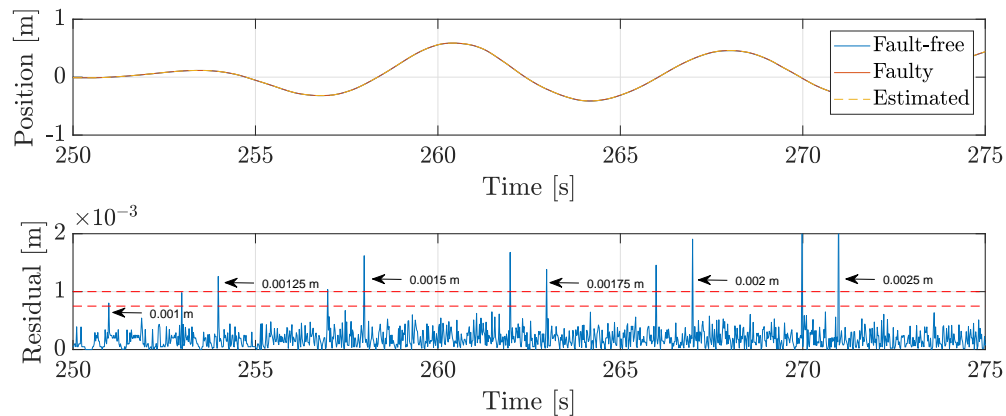
Figure 5-7: Residual for fault type I

at fault sizes between 0.001 and 0.00125 m, Figure 5-8 , it can be seen that the peaks do not always exceed the threshold. Thus it can be concluded that for faults with a magnitude between 0.001 and 0.00125 m are not always detected.

For Fault type I, detection of faults as small as 0.00125 m in step-size can take place. This is a big improvement from the alarm threshold currently defined at 0.05 m. Both the C1 and the C2 sensor can be checked individually with this observer model. All the results shown are done with sensor data from C1 but it is assumed that the results for fault detection are similar for C2.

5-4-3 Fault Type II

The second fault type that is considered is an increase in noise of the signal. Sensor degradation may lead to noisier signals. The noise is modelled as a vector with random integer data points between -1 and 1, which is then multiplied with the magnitude of the noise σ.

When inspecting the raw data, it can be observed that there are some fluctuations on the
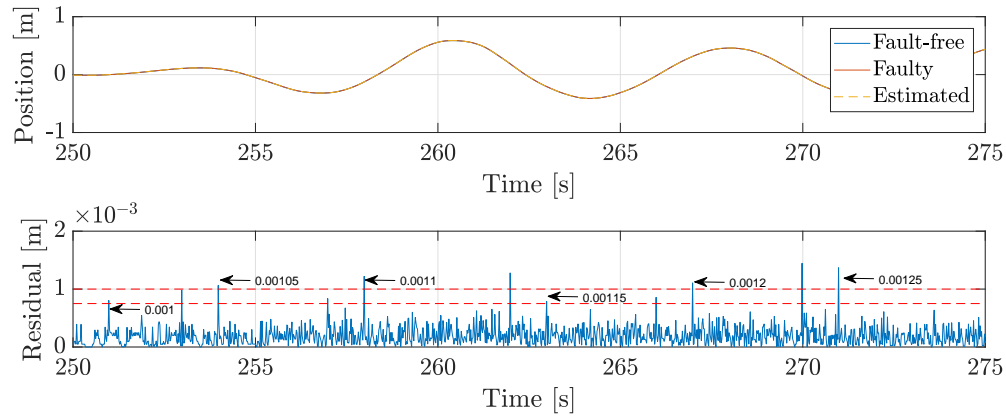
Figure 5-8: Residual for fault type I
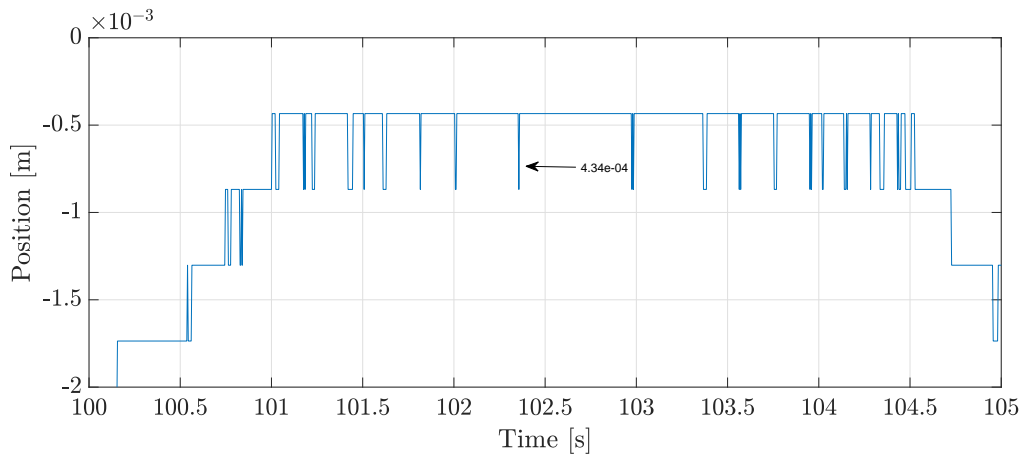
Figure 5-9: Arbitrary section of raw data from the position transducer

measured data of $4.34 \cdot 10^{-4}$ m, Figure 5-9. The residual that is generated for Fault type II should consider raw data in order to make a decision whether the size of the noise exceeds normal conditions.

Thus $\sigma = 4.34 \cdot 10^{-4}$ will be considered normal. Next, the residuals for multiples of σ will be considered, Figure 5-10.

$$\phi = \begin{bmatrix} \sigma \\ 2 \cdot \sigma \\ 3 \cdot \sigma \\ 4 \cdot \sigma \\ 5 \cdot \sigma \\ 6 \cdot \sigma \end{bmatrix} \tag{5-17}$$

It should be noted that the fluctuation as shown in Figure 5-10 are more frequent than shown in Figure 5-9. In this case it is assumed that the frequency has less influence on the residual evaluation in comparison to the size.
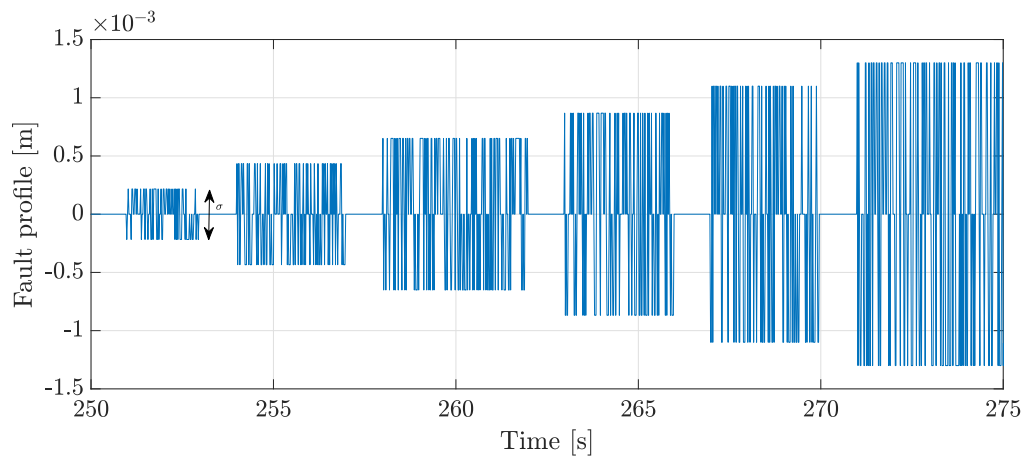
Figure 5-10: Increase in noise Step-like fault profile

Figure 5-11 shows the residual plot for the added noise on the signal. For σ it does not cross the upper threshold thus the normal situation should not lead to a false detection. For the larger values the residual does cross the upper threshold and thus a correct detection takes place.
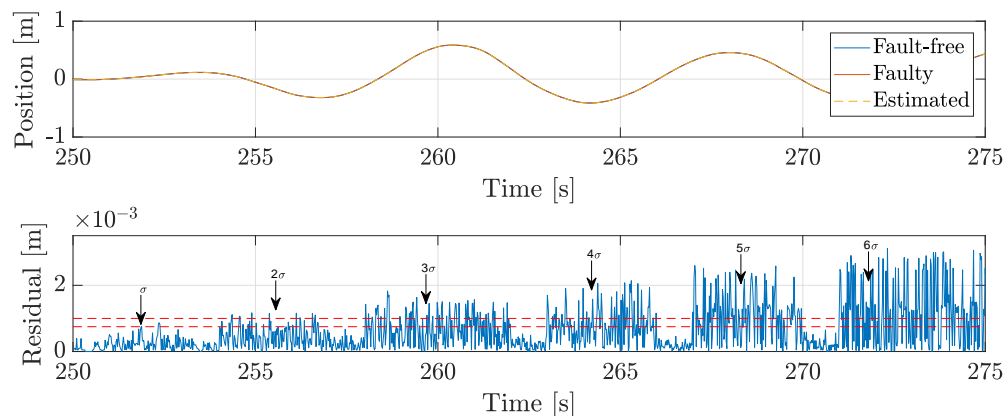
Figure 5-11: Residual for fault type II

5-4-4 Fault Type III

The last fault type is the most difficult to detect because the fault slowly develops over time, which creates the risk that the observer will adjust to the faulty measurement before detection is possible. The fault development profile in Figure 5-12 increases to 0.07 m in about 10 s. This appears to be fast and relatively large when comparing it to the step-like profiles in Section 5-4-2. However for comparison, the step-size of 0.00125 m is modelled as a ramp. From Figure 5-12 it can thus be concluded that the incipient fault develops slower.
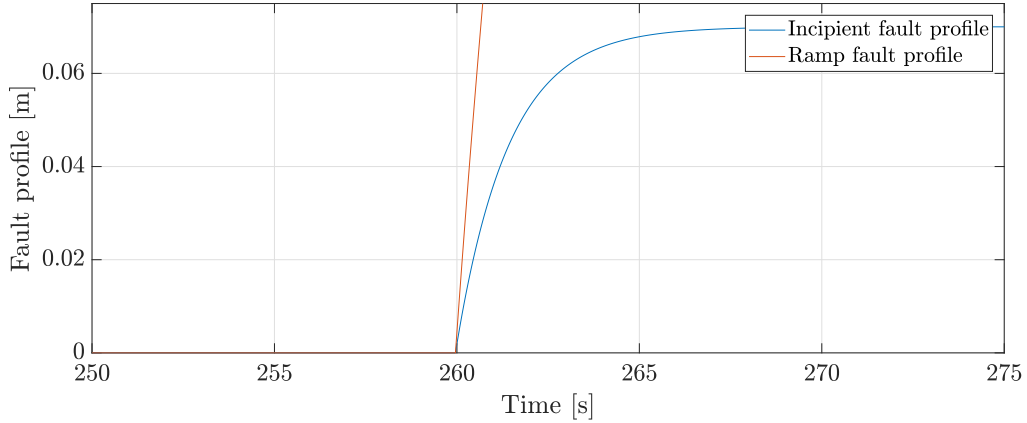
Figure 5-12: Residual for Incipient fault profile

The fault profile that has been chosen is of the following form:

$$\beta(k - k_0) = \begin{cases} 0 & \text{if } k < k_0 \\ 1 - (1 + b)^{-(k-k_0)} & \text{if } k \geq k_0 \end{cases} \tag{5-18}$$

$$fault(k) = \beta(k - k_0) * \phi \tag{5-19}$$

with $b = 1$ and $\phi = 0.07$.

The fault profile in Figure 5-12 results in the residual as shown in Figure 5-13. Detection happens nearly immediately after introduction of the fault. The parameters b and ϕ can be varied. However, to ensure detection, if b is decreased, ϕ has to be increased. This results in fault profiles that have a similar development profile in the first few seconds which will lead to a similar residual.
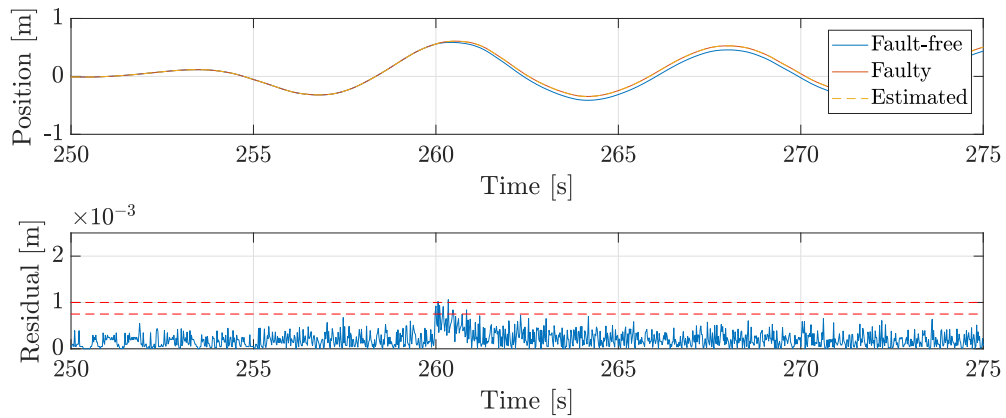
Figure 5-13: Residual for fault type III

The fault is introduced at $k_0 = 259.98$ s. Detection, i.e. when the residual exceeds the upper threshold, takes place at $k_d = 260.06$ s. This is well before the error exceeds 0.05 m thus the detection time is sufficient.

5-5   Residual Generation for R_3

As there are two sensor readings available, a third residual can be generated based on the two measurements. This is already happening in the current Ampelmann Safety Management System (ASMS) to check whether the readings are within range. This can still be used to monitor the health of the sensors. It is expected that the difference between the readings from C1 and C2 are relatively small under normal conditions, though Figure 5-14 shows a different picture. Shown is the difference between the raw measurements from C1 and C2 per cylinder. It can be seen that the error becomes nearly 0.008 m for some cylinder measurements and appears to follow the dynamics of the piston. This could be justified by the fact that the sensors are calibrated differently and thus give different measurement for the same cylinder length.
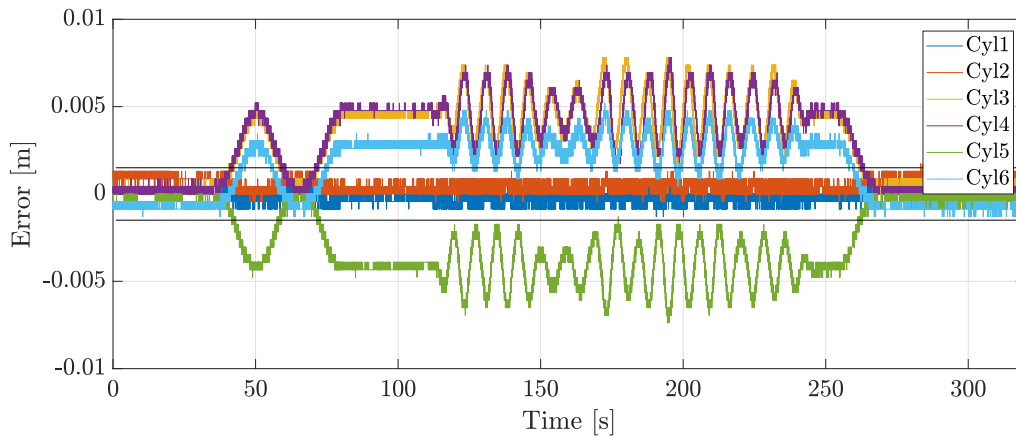
Figure 5-14: Difference between the measurements of C1 and C2 under normal conditions

The black lines in Figure 5-14 show the desired boundaries of $1.5 \cdot 10^{-3}$. It has been assumed that the measurements of C1 are leading. Thus a simple linear model of the following form has been identified in order to reduce the error between C1 and C2 under normal conditions.

$$\hat{C2} = a * C2 + b \tag{5-20}$$

The parameters a and b have been identified by solving the Least Squares (LS) problem. This results in six sets of a and b, one for each set of cylinder sensors. The first part of the data is used for the identification of these parameters. Figure 5-15 represents the error between C1 and $\hat{C2}$ for the second part of the data.

The error signal stays bounded between $[-1.5 \cdot 10^{-3}, 1.5 \cdot 10^{-3}]$ during normal conditions for all cylinders. When a small increasing fault is added to C1, the residual will eventually cross the threshold, Figure 5-16.

Even though no decision can be made about whether the fault occurs in C1 or C2, the evaluation of this residual can lead to a premature warning. No decision can be made about C1 and C2 because a positive fault on C1 gives the same kind of results as a negative fault on C2. However, it does give an improved way to monitor the health of the system. Any faults that are too small to be picked up by the estimator designed in Section 5-4 can be
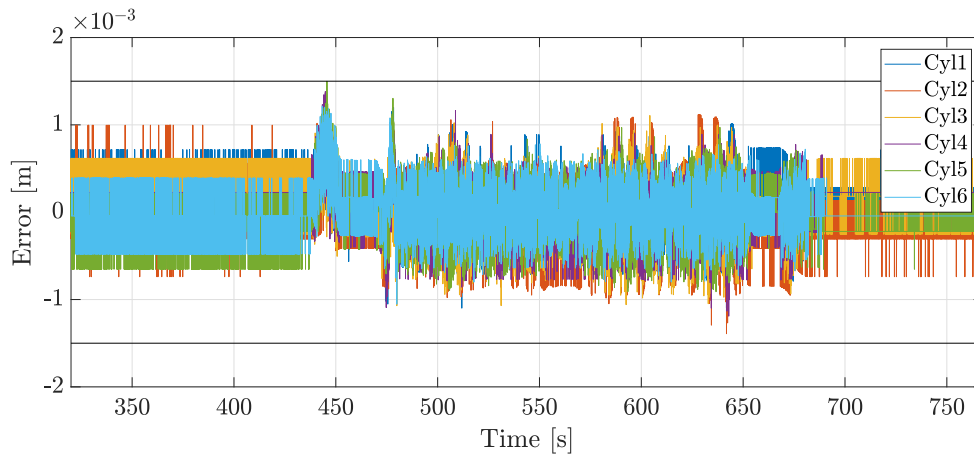
Figure 5-15: Difference between the measurements of C1 and C2 using an LS model for C2
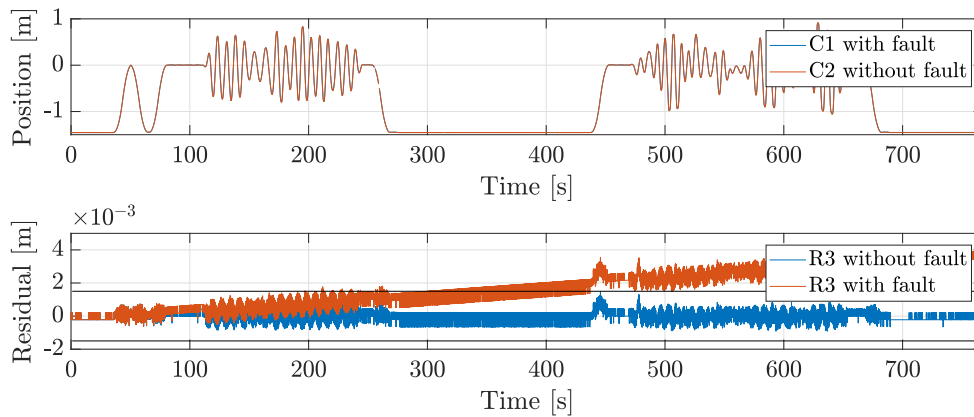
Figure 5-16: Slowly developing fault on C1

detected by monitoring the residual between the measurements. A warning can be given that maintenance is required for one of the sensors when it exceeds 0.0015 m. However, the system can finish operation as long as it does not exceed the critical threshold of 0.05 m.

5-6   The Fault Detection Architecture

All the results from this chapter can be combined into one Fault Detection Architecture, Figure 5-17. The estimator from Section 5-4 corresponds to FDE1 and FDE2. FDE1 and FDE2 check the sensors individually based on the model and observer. All three fault types can be detected using these FDEs, however, the detection does depend on the size of the fault.

FDE3 is similar to the current monitoring system which checks two measurements. However, the residual evaluation is improved by implementing a simple linear model to minimize the error between C1 and C2 when no faults are present. While this FDE cannot make a decision
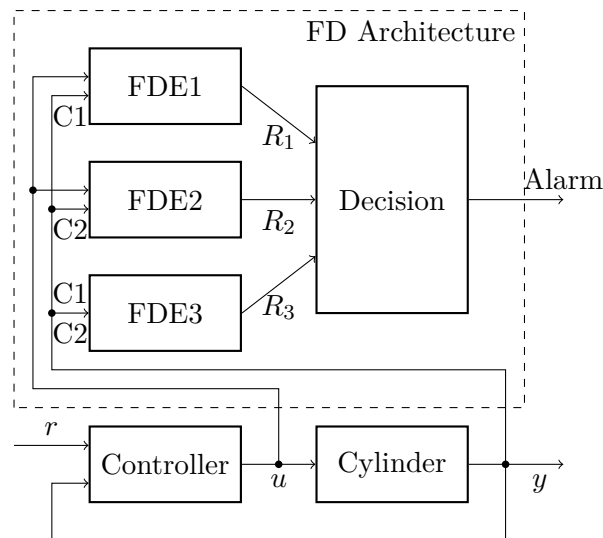
Figure 5-17: Fault Detection Architecture

on the location of the fault, it can give an early warning that maintenance on one of the sensors is required before it exceeds the code black threshold of 0.05 m.

5-7   Summary

The FD architecture designed in this chapter distinguishes between three different sensor fault types, namely step-like, increase in noise and incipient. A model and observer estimate the cylinder lengths which are then compared to the actual measurements. The difference between the measurements and estimates are called residuals. The generated residuals are evaluated for each different fault type. A threshold δ is considered which should separate normal behaviour from faulty behaviour. The threshold is set at $\delta = 0.001$ m. With this threshold, faults with a step size of 0.00125 m can be detected. Detection time is almost immediately after the introduction of the fault. This FDE can be used for each individual sensor without relying on the redundant sensor.

Another check is completed when comparing the readings from both sensors. The error between C1 and C2 does not give a decision on the location of a fault but it can give an early warning that something is going wrong.

All the different estimators can all be combined into one FD architecture to create an extra analytical redundancy measure for the position transducers in the hydraulic cylinders.

Chapter 6

Conclusions and Recommendations

A Fault Detection (FD) strategy for the position transducer has been designed to reduce the occurrence of a code black in the Ampelmann system. Limiting the occurrence of a code black means less downtime for the system. An analytical redundancy measure based on an FD architecture has been given in this thesis. This chapter will synthesize the results and review to what extent the questions posed in Chapter 1 are answered. Finally, recommendations for future research are proposed.

6-1   Conclusion

As indicated in this thesis, the current alarm system still has room for improvement. When it concerns the position transducer, small faults are left undetected by the physical redundancy. This can be solved by adding a third sensor. However, that would increase costs, complexity and components.

This thesis provides an alternative method which uses the concept of analytical redundancy has been explored. A model-based fault detection architecture has been designed to detect different fault types for the position transducer.

Question 1: Can an accurate model of the hydraulic cylinders be derived that can be used for the model-based fault detection method?   In Chapter 4, a linear third order model has been identified based on the mathematical model derived in Chapter 3. The identified model exhibited good results on the estimation capabilities for the cylinder lengths even in open-loop setting. Thus the answer to this question is yes, an accurate model of the hydraulic cylinder that will be used for model-based fault detection can be derived.

Question 2: Using the model from Question 1, can a model-based estimator be designed such that it gives accurate estimates of cylinder lengths?   In Chapter 5, an observer has been added to the model to estimate the cylinder lengths. This observer is sufficiently accurate

to estimate the cylinder lengths. The error between the measured and estimated values is below $7.5 * 10^{-3}$ which is deemed accurate enough. So yes, a model-based estimator can be designed such that it gives accurate estimates of the cylinder lengths.

Question 3: What types of faults can be expected to occur in the sensor that will lead to a difference too big? Three different fault types have been identified in Chapter 5, namely, step-like, an increase in noise and incipient. All three are assumed to indicate sensor degradation or sensor failure. All three are detectable using the model-based estimator from Question 2.

Goal: Increasing reliability of the position measurements and thus reducing downtime of the Ampelmann system by implementing a model-based fault detection method.

Starting off with the implementation of a model-based fault detection method, it has been shown that the goal is achievable and leads to improvement on the detection front when compared to only using physical redundancy. Rather than leaving small faults undetected until a difference of 0.05 m has been reached, faults with a size of 0.00125 m or larger can be detected. This detection process will lead to better use of the redundant sensor.

6-2 Recommendations for Further Research

Based on the results developed throughout this thesis, there are several recommendations for future areas of research related to this problem.

- The proposed FD strategy should be implemented in the software to test whether detection occurs. In the software, a fault signal can be added to the measured signal. This should be picked up by evaluating the residuals and then result in a warning from the system.

- The influence of incorrect position feedback on the control signal has not been considered. It was assumed that this influence is negligible. However, to ensure that this is indeed the case, tests should be executed in order to check the dependence of incorrect feedback from the position transducer on the residual analysis for fault detection.

- The system considered in this thesis is the Ampelmann E-type. A similar strategy can be designed for the Ampelmann A-type by following the approach that this thesis employed for the Ampelmann E-type.

Furthermore, this thesis has delivered insights which can be used for future research on Fault Detection, Fault Tolerant Control and predictive maintenance.

- Fault Detection is not limited to only sensor faults. It can be extended to actuator faults and process faults. Leakages in the cylinder or servo-valve can be considered as actuator faults.

- A different approach to estimate the lengths of the cylinders is to approach the problem from the heaxpod point of view. This would require a model of the hexapod and the assumption that five out of six measurements are correct. However, it can lead to a solution in which only one sensor is required for detection and accommodation.

- The FD forms a basis for Fault Tolerant Control (FTC). If the size and location of the fault are known, rather than switching to the redundant component, the controller can accommodate for the fault leading to a FTC system.

- The detection of incipient faults can lead to more insights for predictive maintenance.

The findings of this study can be used to gather more knowledge about the health of one specific sensor in the system. The results for the position transducer are very promising, therefore, the knowledge on how to design an FD architecture for one sensor can be extended to other components in the Ampelmann system. For less critical sensors which are not redundant, it can offer an additional check without needing the extra components.

Inverse and Forward Kinematics

A-1 Inverse Kinematics

In Figure A-1 the relevant coordinate systems and vectors for the Stewart platform are shown. The three important reference frames are: O^t, local reference frame for the top platform, O^b, local reference frame for the bottom platform and O^f, the inertial reference frame. In Figure A-1a, the vectors $\mathbf{x}$ and $\mathbf{x}_s$ are shown. They denote the translations and rotations of the top and bottom platform respectively to the inertial reference frame O^f. Considering the bottom frame, in (A-1) the translations and rotations are defined by a translation vector $\mathbf{c}_b^f$, see Figure A-1b, and a rotation vector $\mathbf{\Phi}_b^f$ from base frame to inertial reference frame. Where the rotations φ, θ and ψ are around the local reference frame. For the top frame $\mathbf{x}$ can be written in the same way but with subscript t.

$$
\mathbf{x}_s = \begin{bmatrix} \mathbf{c}_b^f \\ \mathbf{\Phi}_b^f \end{bmatrix} = \begin{bmatrix} x \\ y \\ z \\ \varphi \\ \theta \\ \psi \end{bmatrix}
\tag{A-1}
$$

Actuator Lengths

Now to determine the actuator lengths, the Euler transformation matrix needs to be defined. It can be defined by the rotations around the three axes:

$$
R_x(\varphi) = \begin{bmatrix} 1 & 0 & 0 \\ 0 & \cos\varphi & \sin\varphi \\ 0 & -\sin\varphi & \cos\varphi \end{bmatrix}, R_y(\theta) = \begin{bmatrix} \cos\theta & 0 & -sin\theta \\ 0 & 1 & 0 \\ \sin\theta & 0 & \cos\theta \end{bmatrix}, R_z(\psi) = \begin{bmatrix} \cos\psi & \sin\psi & 0 \\ -\sin\psi & \cos\psi & 0 \\ 0 & 0 & 1 \end{bmatrix}
\tag{A-2}
$$
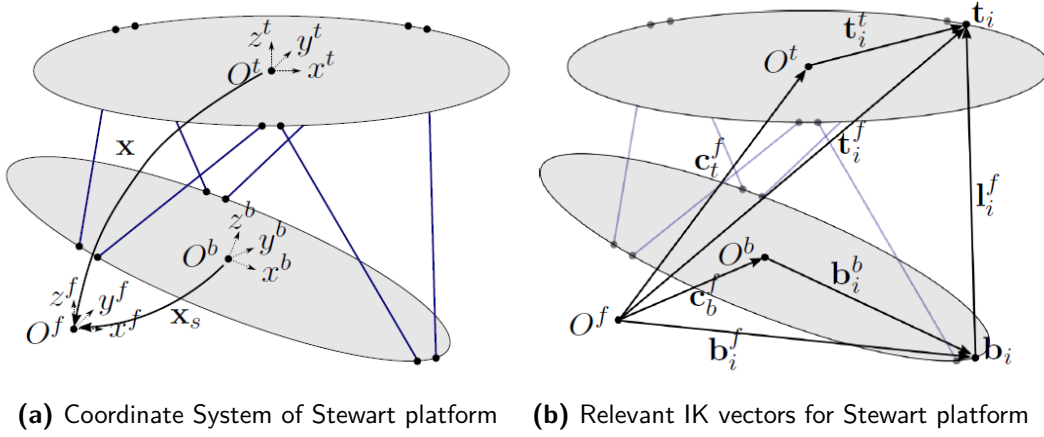
(a) Coordinate System of Stewart platform   (b) Relevant IK vectors for Stewart platform

Figure A-1: The Stewart platform [4]

As rotations are not commutative, the order in which they are applied is of importance [13]. In accordance with the Octans motion sensor and from [1, 3], the order of rotation should be first yaw, then pitch and at last roll. Hence it follows for the bottom frame that:

$$R_b^f(\mathbf{\Phi}_b^f) = R_z(\psi)R_y(\theta)R_x(\varphi) = \bar{R}_b \tag{A-3}$$

The notation $\bar{R}_b$ is used for simplicity. This is the rotation martrix which describes the rotation from bottom frame to inertial reference frame. It can be used to transform the position of any bottom platform gimbal $\mathbf{b}_i^b$ from its respective coordinate system O^b to the inertial frame coordinate system O^f.

$$\mathbf{b}_i^f = \bar{R}_b\mathbf{b}_i^b + \mathbf{c}_b^f \tag{A-4}$$

where $\mathbf{b}_i^b$ is the coordinates of the i-th bottom gimbal in its local reference frame and $\mathbf{b}_i^f$ the coordinates of the i-th gimbal in the inertial reference frame. Similarly, any top gimbal $\mathbf{t}_i^f$ can be described in O^f:

$$\mathbf{t}_i^f = \bar{R}_t\mathbf{t}_i^t + \mathbf{c}_t^f \tag{A-5}$$

with its relative position $\mathbf{x}$ denoted by:

$$\mathbf{x} = \begin{bmatrix} \mathbf{c}_t^f \\ \mathbf{\Phi}_t^f \end{bmatrix} \tag{A-6}$$

Now to determine the length of each actuator, it can be defined as the line between a point on the top and bottom platform. This can be defined as a gimbal pair i. Then for each i-th actuator the length is defined as follows:

$$\mathbf{l}_i^f = \mathbf{t}_i^f - \mathbf{b}_i^f \tag{A-7}$$

Note that to determine the lengths between the two gimbal points, the gimbal points need to be defined in the same reference frame, O^f in this case. The length, ℓ, and direction, $\mathbf{z}$, are then defined as follows:

$$\ell_i = \|\mathbf{t}_i^f - \mathbf{b}_i^f\| \tag{A-8}$$

$$\mathbf{z}_i = \frac{\mathbf{l}_i^f}{\ell_i} \tag{A-9}$$

The reference length can then be determined by subtracting the neutral cylinder length from (A-8).

$$r_i = \ell_i - l_0 \tag{A-10}$$

The neutral cylinder length is defined as the cylinder length when the platform is at half its maximum heave displacement.

Actuator Velocities

As for the velocities, a transformation can be made between the actuator velocities $\dot{\mathbf{l}}$ and platform velocities $\dot{\mathbf{x}}$ and $\dot{\mathbf{x}}_s$. The Jacobian relates the actuator velocities with the platform velocities [4]. However the term Jacobian is not precise as it is not the partial derivative of a vector but a set of velocities as a function of another set of velocities [14].

$$\mathbf{J} = \begin{bmatrix} \mathbf{z}_1^T & (\bar{\mathbf{R}}_t^b \mathbf{t}_1^f \times \mathbf{z}_1)^T \\ \vdots & \vdots \\ \mathbf{z}_6^T & (\bar{\mathbf{R}}_t^b \mathbf{t}_6^f \times \mathbf{z}_6)^T \end{bmatrix} \tag{A-11}$$

where $\bar{R}_t^b$ is the transformation matrix from O^t to O^b. As the Jacobian defines the kinematics of the Stewart platform, it is the same from both the bottom and top perspective.

Now to define the relationship between the actuator velocities and the platform velocities, first the bottom platform is considered fixed. The actuator velocities as result of the top platform velocities can be defined using the Jacobian:

$$\dot{\mathbf{l}}_t = \mathbf{J}\dot{\mathbf{x}} \tag{A-12}$$

Next the top platform is considered to be fixed to determine the actuator velocities as result from the bottom platform velocities.

$$\dot{\mathbf{l}}_b = -\mathbf{J}\dot{\mathbf{x}}_s \tag{A-13}$$

Combining (A-12) and (A-13), the total actuator velocity can be found. It is defined as the sum of both: Hence the total actuator velocity is:

$$\mathbf{i} = \mathbf{i}_t + \mathbf{i}_b$$
$$= \mathbf{J}(\dot{\mathbf{x}} - \dot{\mathbf{x}}_s) \tag{A-14}$$

This concludes the IK problem for finding the actuator lengths and velocities.

A-2   Forward Kinematics

The Forward Kinematics (FK) problem is used to find the orientation of the top and bottom platform relative to each other given the lengths and direction of the six actuators. This results in solving the following kinematic equation:

$$\ell_i^2 = \|\mathbf{t}_i^b - \mathbf{b}_i^b\|^2 \tag{A-15}$$

which is an analytical way of describing the placing of the top rigid body such that six given points lie on six given spheres which are fixed to the base rigid body. However solving this, is considered a difficult problem due to the large number of complicated constraints [15]. There are 30 non-linear algebraic equations that need to be solved simultaneously. Large computational powers are required to solve this, furthermore at most 40 solution (including complex) can be found [1]. It can however be solved numerically using a Newton Rhapson (NR) iteration method. The general NR iteration solves for $f(x) = 0$ according to the following scheme:

$$x_{n+1} = x_n - [f'(x_n)]^{-1} f(x_n), \quad n = 0, 1, ... \tag{A-16}$$

where $f(x_n)$ has to be defined so that it is applicable to the Stewart platform. If (A-15) needs to be solved then it follows that:

$$f_i(\mathbf{x}) = \mathbf{l}_i^T \mathbf{l}_i - \ell_i^2 \tag{A-17}$$

should be solved for 0. Where $\mathbf{x}$ is the position and orientation of the top platform. Hence this results in:

$$\mathbf{x}_{n+1} = \mathbf{x}_n - [\tfrac{\partial \mathbf{f}(\mathbf{x}_n)}{\partial \mathbf{x}_n}]^{-1} \mathbf{f}(\mathbf{x}_n), \quad n = 0, 1, ... \tag{A-18}$$

where $\mathbf{f}(\mathbf{x}) = \begin{bmatrix} f_1(\mathbf{x}) & f_2(\mathbf{x}) & ... & f_6(\mathbf{x}) \end{bmatrix}^T$ as to include all six actuators. For on-line control, it is important that only the correct solution is picked and that the solution is fast enough for real-time implementation. For the Ampelmann system, the NR method converges within a few iteration steps.

Bibliography

[1] D. C. Salzman, *Development of the Acces System for Offshore Wind Turbines.* PhD thesis, Delft University of Technology, 2010.

[2] M. Jelali and A. Kroll, *Hydraulic Servo-systems.* Springer London, 2003.

[3] A. van Leer, "Motion control enhancements for the ampelmann system," Master's thesis, Delft University of Technology, 2011.

[4] K. Lie, "Inverse dynamics control for the ampelmann system," Master's thesis, Delft University of Technology, 2017.

[5] M. Blanke, M. Kinnaert, J. Lunze, and M. Staroswiecki, *Diagnosis and Fault-Tolerant Control.* Springer, 2015.

[6] E. Fichter, "A stewart platform- based manipulator: General theory and practical construction," *The International Journal of Robotics Research*, vol. 5, no. 2, pp. 157–182, 1986.

[7] N. van der Steen, "Ship motion prediction for the ampelmann system," Master's thesis, Delft University of Technology, 2016.

[8] J. de Vriend, J. van Rooijen, and J. Flohil, "Dpe project: Controller improvements. tuning and performance of the a-type." Presentation. Internal documentation Ampelmann B.V., 2016.

[9] D. Maneetham and N. Afzulpurkar, "Modeling, simulation and control of high speed nonlinear hydraulic servo system," *World Journal of Modelling and Simulation*, 2010.

[10] M. Verhaegen and V. Verdult, *Filtering and System Identification: A Least Squares Approach.* Cambridge University Press, 2012.

[11] R. M. Ferrari, T. Parisini, and M. M. Polycarpou, "A fault detection and isolation scheme for nonlinear uncertain discrete-time sytems," in *2007 46th IEEE Conference on Decision and Control*, IEEE, 2007.

[12] R. M. Ferrari, T. Parisini, and M. M. Polycarpou, "A robust fault detection and isolation scheme for a class of uncertain input-output discrete-time nonlinear systems," in *2008 American Control Conference*, IEEE, jun 2008.

[13] S. Koekebakker, *Model Based Control of a Flight Simulator Motion System.* PhD thesis, Delft University of Technology, 2001.

[14] A. Weterings, "Robust controller design of two coupled hexapods for k&c test system," Master's thesis, Delft University of Technology, 2010.

[15] R. M. Murray, S. S. Sastry, and L. Zexiang, *A Mathematical Introduction to Robotic Manipulation.* CRC Press, Inc., 1994.

Glossary

List of Acronyms

ASMS	Ampelmann Safety Management System
DoF	Degrees of Freedom
FD	Fault Detection
FDEs	Fault Detection Estimators
FK	Forward Kinematics
FTC	Fault Tolerant Control
HSS	Hydraulic Servo System
HPU	Hydraulic Power Unit
IK	Inverse Kinematics
LS	Least Squares
LQR	Linear Quadratic Regulator
MRU	Motion Reference Unit
NR	Newton Rhapson
PLC	Programmable Logic Controller
PTA	Piston Type Accumulator
VAF	Variance Accounted For

List of Symbols

$\mathbf{\Phi}_b^f$	Rotational position bottom platform in O^f
α	Parameter which determines influence of piston velocity on Pressure dynamics
$\bar{R}_b$	Rotation matrix from bottom frame to inertial frame
β	Parameter which determines influence of Load Pressure on Pressure dynamics
$\ddot{x}$	Translational acceleration for surge [m/s^2]
$\ddot{y}$	Translational acceleration for sway [m/s^2]
$\ddot{z}$	Translational acceleration for heave [m/s^2]
δ	Threshold for fault detection [m]
$\dot{\psi}$	Rotational velocity for yaw [rad/s]
$\dot{\theta}$	Rotational velocity for roll [rad/s]
$\dot{\varphi}$	Rotational velocity for pitch [rad/s]
$\dot{l}$	Velocity of Cylinder [m/s]
$\dot{l}_{ctrl}$	Control speed for Cylinder [m/s]
$\dot{x}$	Translational velocity for surge [m/s]
$\dot{y}$	Translational velocity for sway [m/s]
$\dot{z}$	Translational velocity for heave [m/s]
γ_1	Parameter which determines the influence of the input on the piston dynamics
γ_2	Parameter which determines the influence of the input on the pressure dynamics
$\hat{\theta}$	Estimated parameter vector
$\dot{\mathbf{l}}$	Cylinder velocity [m/s]
$\dot{\mathbf{x}}$	Top platform velocity [m/s]
$\dot{\mathbf{x}}_s$	Bottom platform velocity [m/s]
$\mathbf{b}_i^b$	Position of the i-th gimbal in the bottom frame
$\mathbf{c}_b^f$	Translational position platform in O^f
$\mathbf{t}_i^f$	Position of the i-th gimbal in the top frame
$\mathbf{x}$	Position top platform in O^f
$\mathbf{x}_s$	Position bottom platform in O^f
μ_v	Viscous friction coefficient
ϕ	Oil flow into Cylinder [m/s^3]
ϕ_L	Load oil flow [m/s^3]
ϕ_{bot}	Oil flow into bottom chamber [m/s^3]
ϕ_{rod}	Oil flow into rod-side chamber [m/s^3]
ψ	Rotation for yaw [rad]
ρ	Oil density [kg/m^3]
σ	Parameter for noise [m]
θ	Parameter vector
θ	Rotation for roll [rad]
φ	Rotation for pitch [rad]

a	Identifiable parameter
$A_v(x_m)$	Spool position dependent valve area [m^2]
b	Identifiable parameter
C_d	Discharge coefficient
c_s	Stribeck velocity
F_{c0}	Parameter for Coulomb friction
F_{fr}	Friction Force in Cylinder [N]
F_{s0}	Parameter for static friction
k	Actuator stiffness [N/m]
k_0	Time index of fault occurence
L	Observer gain
l	Position of Cylinder [m]
m	Load mass [kg]
O^b	Local reference frame of bottom platform
O^f	Inertial reference frame
O^t	Local reference frame of top platform
P_1	High Pressure [bar]
P_2	Low Pressure [bar]
P_L	Load Pressure [bar]
P_S	Supply pressure [bar]
P_T	Return Pressure [bar]
P_{bot}	Pressure in bottom chamber of Cylinder [bar]
P_{rod}	Pressure in rod-side chamber of Cylinder [bar]
Q	Matrix for LQR Control for the state
R	Matrix for LQR Control for the input
R_1	Fault detection residual 1
R_2	Fault detection residual 2
R_3	Fault detection residual 3
U	Data vector for input
x	Translation for surge [m]
X_1	Data vector for x_1
X_2	Data vector for x_2
X_3	Data vector for x_3
x_m	Spool position [%]
y	Translation for sway [m]
z	Translation for heave [m]